Published in final edited form as:

Hippocampus. 2014 August ; 24(8): 943–962. doi:10.1002/hipo.22282.

N-cadherin regulates molecular organization of excitatory and inhibitory synaptic circuits in adult hippocampus *in vivo*

Jessica S. Nikitczuk, **Shekhar B. Patil**, **Bridget A. Matikainen-Ankney**, **Joseph Scarpa**, **Matthew L. Shapiro**, **Deanna L. Benson**[#], and **George W. Huntley**[#]

Fishberg Department of Neuroscience, Friedman Brain Institute and The Graduate School of Biomedical Sciences, The Icahn School of Medicine at Mount Sinai, 1470 Madison Avenue, New York, NY 10029

[#] These authors contributed equally to this work.

Abstract

N-cadherin and β-catenin form a transsynaptic adhesion complex required for spine and synapse development. In adulthood, N-cadherin mediates persistent synaptic plasticity, but whether the role of N-cadherin at mature synapses is similar to that at developing synapses is unclear. To address this, we conditionally ablated N-cadherin from excitatory forebrain synapses in mice starting in late postnatal life and examined hippocampal structure and function in adulthood. In the absence of N-cadherin, β-catenin levels were reduced, but numbers of excitatory synapses were unchanged, and there was no impact on number or shape of dendrites or spines. However, the composition of synaptic molecules was altered. Levels of GluA1 and its scaffolding protein PSD95 were diminished and the density of immunolabeled puncta was decreased, without effects on other glutamate receptors and their scaffolding proteins. Additionally, loss of N-cadherin at excitatory synapses triggered increases in the density of markers for inhibitory synapses and decreased severity of hippocampal seizures. Finally, adult mutant mice were profoundly impaired in hippocampal-dependent memory for spatial episodes. These results demonstrate a novel function for the N-cadherin/β-catenin complex in regulating ionotropic receptor composition of excitatory synapses, an appropriate balance of excitatory and inhibitory synaptic proteins and the maintenance of neural circuitry necessary to generate flexible yet persistent cognitive and synaptic function.

Keywords

catenins; cell adhesion molecules; seizures; transgenic; water maze

Introduction

N-cadherin and β-catenin compose part of a transcellular, homophilically-binding adhesive complex that has multifaceted roles in mammalian brain development. At early stages, N-

Corresponding Authors: Dr. George W. Huntley, george.huntley@mssm.edu, Tel: 212-824-8981, Fax: 646-537-9583 or Dr. Deanna L. Benson, deanna.benson@mssm.edu, Tel: 212-824-8974, Fax: 646-537-9583.

CONFLICT OF INTEREST STATEMENT: The authors declare no known conflicts of interest.

cadherin/β-catenin linkage to actin generates traction important for neuronal and axonal growth cone migration, and homophilic adhesion contributes to axonal target recognition (Yamagata and Sanes 1995; Poskanzer et al. 2003; Kadowaki et al. 2007). At later stages, N-cadherin becomes concentrated at excitatory synapses (Yamagata et al. 1995; Fannon and Colman 1996; Benson and Tanaka 1998), where together with ß-catenin, it plays a significant role in generation of synapses, elaboration of dendrites, morphogenesis of dendritic spines and maturation of presynaptic functional properties (Togashi et al. 2002; Bamji et al. 2003; Yu and Malenka 2003; Bozdagi et al. 2004; Jungling et al. 2006; Bekirov et al. 2008).

Studies of cultured hippocampal neurons show that at early stages, when synapses are first assembling, acutely interferring with cadherin adhesion directly (using dominant-negative entities) or indirectly (by depolymerizing the actin network leading to dispersion of synaptically-clustered N-cadherin) significantly disrupts apposition of pre- to-postsynaptic membranes (Zhang and Benson 2001; Togashi et al. 2002; Bozdagi et al. 2004). In contrast, after synapses have become established, these same manipulations have little or no effect on the structural integrity of pre- to-postsynaptic membrane apposition (Zhang and Benson 2001; Bozdagi et al. 2004), suggesting that after a certain period of development, cadherins become dispensible for synaptic adhesion necessary for holding pre- and postsynaptic membranes together. Nevertheless, the N-cadherin/β-catenin complex remains a prominent component of excitatory forebrain synapses throughout adulthood. Thus, it is uncertain what N-cadherin contributes to mature synaptic circuit structure and function, particularly *in vivo*. Recent studies have shown that mature hippocampal CA1 synapses lacking N-cadherin display significant deficits in long-term potentiation (LTP) and are unable to sustain the dendritic spine enlargement that accompanies LTP, but have no apparent defects in long-term depression (LTD) or changes in properties of baseline synaptic neurotransmission (Bozdagi et al. 2010). The anatomical and/or molecular underpinnings and the behavioral significance of such selective synaptic deficits are unknown. Based predominantly on cell culture models of N-cadherin/β-catenin function, such deficits could reflect altered synapse morphology, turnover and stability (Mendez et al. 2010) or they could result from changes in the composition of receptors and anchoring proteins important for dynamic synaptic neurotransmisson (Coussen et al. 2002; Tai et al. 2008).

Here, we investigated these possibilities *in vivo* using a conditional genetic deletion strategy that eliminates N-cadherin and reduces levels of β-catenin at hippocampal and other forebrain synapses starting in late postnatal life. In contrast to early development, N-cadherin/β-catenin complex is not required for maintaining dendrite, spine or synapse number or morphology in adult hippocampus. Instead, the complex becomes crucial for the selective maintenance of levels and localization of GluA1 and its scaffolding protein PSD95, without affecting other AMPA receptor (AMPAR) or NMDA receptor (NMDAR) subunits or their scaffolding proteins. Moreover, GABAergic synapse markers are elevated in hippocampus while seizure severity is significantly reduced, suggesting that inhibitory circuitry is functionally enhanced by the loss of N-cadherin. Together, these changes in the molecular architecture and physiology of mature excitatory and inhibitory circuits likely contribute to significant impairment in spatial memory displayed by the conditional knockout (cKO) mice.

Materials and Methods

Animals

Details of the generation and characterization of the N-cadherin cKO mice were reported previously (Bozdagi et al. 2010). Briefly, the cKO mice were generated on a C57Bl6 background by crossing a line of LoxP-flanked (floxed) N-cadherin mice (Kostetskii et al. 2005) with an αCaMKII-Cre driver line of mice (Camk2a-Cre; T29-1 line; Jackson Labs (Tsien et al. 1996)). In this line, Cre recombinase is expressed in principal neurons of DG, CA1 and CA3 (Tsien et al. 1996); Allen Brain Atlas). Treatment and use of all animals were strictly in accordance with animal welfare protocols approved by Mount Sinai's Institutional Animal Care and Use Committee and followed guidelines established by the NIH.

Stereological analysis of neuron and synapse density

Adult (5 mo-old) cKO or floxed control mice (n=3 male mice per genotype) were perfused with 2% paraformaldehyde/2% glutaraldehyde and embedded in Lowicryl as described previously (Elste and Benson 2006; Bozdagi et al. 2010). Stereological methods were used to estimate neuron density, synapse density and to calculate number of synapses-per-neuron in CA1 according to methods outlined previously (Kleim et al. 1996). Briefly, neuron density in CA1 was estimated using Neurolucida software (MBF Biosciences) in which the double-dissector method was applied to serial 1 μm-thick Lowicryl-embedded sections stained with methylene blue (Geinisman et al. 1996). Synapse density in CA1 was estimated by applying the double-dissector method to electron-micrographs of CA1 stratum radiatum obtained from serial ultrathin sections (70 nm) cut from the same series of semi-thin sections used to estimate neuron density. The number of synapses-per-neuron was then calculated by dividing the number of synapses per cubic volume by the number of neurons per cubic volume.

Dendrite and spine morphological analysis

Morphometric analysis of apical dendritic branching and spine density and morphology was determined from young adult (3-6 mo) male cKO (n=4) or floxed control (n=3) mice. Mice were perfused intracardially with 4% paraformaldehyde and 250 μm-thick sections through hippocampus were cut on a vibratome. Pyramidal neurons in CA1, CA3 and dentate gyrus granule neurons (8-18 neurons per region per genotype) were then intracellularly filled with 5% Lucifer Yellow delivered iontophoretically through a glass micropipette as described (Radley et al. 2006). Total apical dendritic length and a Scholl analysis of apical dendritic branching was determined for CA1 pyramidal neurons using NeuroExplorer software (MBF Biosciences). Apical dendritic spine density/morphology analysis was carried out on CA3 and DG neurons as done previously for adult N-cadherin cKO and floxed CA1 neurons (Bozdagi O *et al.* 2010), with some additional analyses of all three subregions. Apical dendritic segments (9-15 per neuron) were imaged on a Zeiss 510 confocal microscope. Low-power (40×) image stacks through the soma and dendritic tree were acquired initially. Three concentric circles centered on the soma were then drawn with radii of 50, 100 or 150 μm. These were used as a guide for high-resolution imaging (100×) of secondary and tertiary apical dendrites that intersected the circles. These high-resolution image stacks were deconvolved and analyzed using an automated program (NeuronStudio) that classifies

subtypes of spines (stubby, thin, mushroom) based on several parameters including spine head-to-neck ratio and spine-head diameter (Wearne et al. 2005; Rodriguez et al. 2006). The detection and classification algorithms were validated in the same dataset by visual inspection of the spines analyzed.

Immunoblotting

Immunoblotting was carried out on whole-hippocampal lysates from cKO or floxed control tissue (n=3 mice per genotype of either sex) as described (Bozdagi et al. 2010), or on synaptoneurosomes isolated from whole-hippocampus (n=3 male mice per genotype) as described (Chen et al. 2011). All analyses were carried out on adult animals (3-6 mo-old) except for the developmental analysis shown in Figure 2, the ages for which are indicated in the legend. Synaptoneurosomes were prepared from hippocampi that were homogenized in lysis buffer containing 10 mM HEPES, 2 mM EDTA, 2 mM EGTA, 0.5 mM DTT, phosphatase and protease inhibitor cocktails (Sigma) using a glass-Teflon homogenizer. To one-fifth volume of the homogenates, NaCl was added to a final concentration of 0.2 M, incubated for 30 minutes, then centrifuged for 30 minutes. Supernatants were sequentially filtered through a 100 μm nylon-mesh filter followed by a 5 μm nitrocellulose filter. Filtrates were centrifuged at 1,000*g* for 10 minutes and pellets were dissolved in lysis buffer. Protein concentrations were determined using Bio-Rad protein assay (Bio-Rad Laboratories, Hercules, CA). 10 μg protein from each animal was resolved simultaneously by SDS-PAGE and transferred to Immune-Blot PVDF membranes (Bio-Rad) by Semi-Dry electroblotting. Membranes were blocked for 1 hour in 10% NBCS/TBST at room temperature and then incubated in primary antibodies overnight at 4°C. The primary antibodies or sera used in this analysis were directed against the following: N-cadherin (BD Transduction Labs, 1:2000); β-catenin (Millipore, 1:7500); GluA1 (Millipore, 1:7500); GluA2 (BD Pharmingen, 1:1000); GluN1 (Millipore, 1:2000); GluN2B (Chemicon, 1:1000); gephyrin (Millipore, 1:1000); glutamic acid decarboxylase-65 (GAD65; Millipore, 1:1000); SynCAM-1 (clone 3E1; MBL International, 1:1000); vesicular GABA transporter (VGAT; Synaptic Systems, 1:1000); PSD95 (clone 7E3-1B8; Thermo Scientific, 1:2000); pan-PSD95-family (clone 6G6-1C9; Thermo Scientific, 1:1000); S-SCAM/MAGI-2 (Sigma-Aldrich, 1:5000) and synaptophysin (Sigma-Aldrich, 1:15,000). Antibodies to tubulin (Abcam, 1:1000), GAPDH (Trevigen, 1:25,000) or actin (Millipore, 1:4000) were used as loading controls. For the blots shown in Figs. 2, 6, and 7, membranes were subsequently washed, treated with secondary horseradish peroxidase-labeled antibody for 1 hour at room temperature and washed again. Membranes were then incubated with ECL detection reagents (Thermo Scientific, Pittsburgh, PA) for 30 seconds and exposed to HyBlotCL (Denville Scientific, Denville, NJ) and developed. For the blots shown in Figs. 1 and 8, membranes were washed and treated with fluorophore-conjugated secondary antibodies (DyLight 800, Cell Signaling, and DyLight 680, Pierce) and visualized using a Li-cor Odyssey Clx imaging system (Li-Cor Biosciences). For each primary antibody, levels of immunoreactivity were determined from three independent experiments by film densitometry (ImageJ) in which band intensity of the protein of interest was normalized to that of its loading control within the same lane. Figure 1 verifies the enrichment of two representative postsynaptic proteins (the synaptic cell adhesion molecule SynCAM and PSD95 in the synaptoneurosome preparation in comparison with whole-tissue lysates from wildtype C57Bl6 adult male mice (n=7-9). For the developmental analysis (n=3

mice per timepoint), band intensity at each age was normalized to its loading control, then expressed as a percentage of the average values for the 6 mo-old floxed mice.

Immunofluorescence

Procedures, controls and quantitative analyses have been described in detail previously (Brock et al. 2004; Bozdagi et al. 2010). Experiments were conducted on adult (4-6 mo-old) cKO or floxed mice (n=4-8 mice per genotype, both sexes). All mice were perfused with 4% paraformaldehyde and serial hippocampal sections were cut on a vibratome. Sections were subjected to an antigen retrieval protocol that consisted of incubation in dH_20 for 6.5 min at 37°C followed by incubation in a 0.2N HCl solution containing 1 mg/ml pepsin at 37°C for one hour. Sections were then incubated in one of the following primary antibodies: N-cadherin (1:400); β-catenin (1:500); GluA1 (1:500); GluA2 (1:200); GluN1 (1:1000); PSD95 (clone 7E3-1B8 1:500), GAD65 (1:1000) and gephyrin (1:1500), all from the companies listed above, plus vesicular glutamate transporters (vGluts) 1 and 2 (Millipore, 1:2500). Antibody binding was visualized with Alexa fluorophore-conjugated secondary antibodies (Molecular Probes). Immunofluorescent detection of primary antibody binding was achieved by acquiring images on a Zeiss 510 laser-scanning confocal microscope. Image acquisition parameters were optimized for floxed controls and held constant. Quantitative analysis was conducted by an investigator blinded to genotype. Immunolabeled puncta density and size were determined from 3-6 sections per mouse by thresholding following deconvolution (Metamorph, Molecular Devices). All quantitative values (puncta density and size) for each hippocampal subfield were normalized to floxed control values for that subfield.

Antibody specificity (Table 1)

Table 1 lists the antibodies or sera used in this study. We have verified the specificity of the N-cadherin antibody previously. Briefly, this antibody recognizes L-cells transfected with full-length N-cadherin, but not L-cells transfected with full-length E-cadherin (Brock et al. 2004). Immunoblot analysis of hippocampal or spinal cord lysates shows a single band of the appropriate (~125 kd) molecular mass (e.g. Fig. 2). Additionally, in N-cadherin cKO mice, hippocampal synaptic immunolocalization is abolished and, similarly, there is no labeling found in hippocampal postsynaptic density fractions (Bozdagi et al. 2010). Previous studies have shown that the PSD95 antibody (clone 7E3-1B8) is strongly reactive to PSD95, has minimal cross-reactivity to PSD93, and no cross-reactivity to SAP97 or to SAP102 (Sans et al. 2000). The antibody to pan-PSD95 family members (clone 6G6-1C9, used only for the blots shown in Fig. 1) is strongly reactive to SAP97, PSD93 and PSD95 but displays no reactivity to SAP102 (Sans et al. 2000). The antibodies or sera used as synaptic markers (postsynaptic scaffolding molecules, SynCAM-1, GluRs, GAD65, gephyrin, VGAT, and synaptic vesicle markers) all produced immunolabeling patterns and/or showed expected bands of the appropriate molecular mass as described previously by others under similar experimental conditions. Controls for non-specific binding of the secondary antibodies included processing sections immunofluorescently as described except for omitting the primary antibodies. No specific labeling was observed under these conditions.

Kainic acid injection and seizure behavior

Wildtype mice (n=3 males, 3-4 mo-old) or cKO mice (n=4 males, 3-4 mo-old) were injected with kainic acid (Sigma; 35 mg/kg IP in 0.9% saline) or saline alone (vehicle control). Behavioral manifestations of seizure activity were observed in real time over a 3-hr period using an adaptation (McKhann et al. 2003) of a previously described behavioral scale (Racine 1972): 0= no behavioral abnormalities; 1 = immobility; 2 = forelimb and/or tail extension; 3 = repetitive scratching, circling, or head bobbing (automatisms); 4 = intermittant forelimb clonus, rearing, and/or falling; 5 = continuous repetition of stage 4; and 6 = whole-body tonic–clonic convulsions. For each animal, the 3-hr observation period was divided into 10-min bins; the highest behavioral score during each 10-min bin was then plotted for that bin as a pseudo-colored heatmap. A mean cumulative seizure score over the 3-hr observation period was obtained for animals of each genotype, and comparisons of these mean scores between genotypes were evaluated using an unpaired t-test.

Behavioral tests for spatial reference memory

A six-arm radial water maze was used to test adult (4-6 mo-old) cKO (n=13) and floxed control mice (n=11) of either sex for spatial reference memory using procedures that followed previous descriptions (Fletcher et al. 2007; Shirvalkar et al. 2010).

Apparatus—The radial arm water maze consisted of a white circular tank (170cm diameter, 62.5cm height) with six arms, formed with equally spaced triangular dividers projecting radially from the center, extending 55.5cm into the maze. The tank was filled with water to a depth of 48cm, made opaque with white tempura paint (Dick Blick Arts), and maintained at a temperature of 22-24°C. A clear acrylic escape platform (25×25 cm^2) was placed at the end of one arm adjacent to the tank wall and submerged 1cm. Different objects were placed on the walls surrounding the pool to allow for spatial orientation within the maze, and were held constant for the remainder of the experiment.

Pretraining—Mice underwent two-three days of cue-approach pretraining during which the platform was not submerged and a visible cue was suspended ~6 inches above the platform. Location of the visible cue and the platform was changed at the start of each cue-approach pretraining day. Once the mouse was able to locate the visible platform in under 12 seconds for four consecutive trials, the mouse moved on to the training phase.

Training—The purpose of training was to ensure that the mouse could locate a hidden platform. In the training phase, the platform was submerged and there was no visible cue suspended above the platform. Location of the platform was changed at the start of each cue-approach training day. For both training and subsequent testing in the tasks, the platform was placed at the end of a pseudorandomly chosen arm (goal arm). The criteria required for a mouse to move on to the testing phase was defined as having the ability to locate the hidden platform in under 12 seconds for four consecutive trials.

Testing: Matching-to-place task—At the beginning of each of 6 days of testing, a submerged escape platform was placed at the end of a pseudorandomly chosen goal arm where it remained for each of the 8 trials of that day. In each trial, a mouse was placed in the

water facing the end of a pseudorandomly chosen start arm and could escape the water by finding the position of the submerged platform. The mouse was given one initial trial (the sample trial) to find the location of the platform by trial-and-error. Optimum performance required that the mouse learn the location of the escape platform on the sample trial (trial 1) in order to swim directly to it on subsequent match trials (trials 2-8, intertrial interval 70 sec). The location of the escape platform was changed for each daily testing session, requiring the mice to learn the position of a different goal arm each day. Mice were given 60 seconds per trial to find the platform. If the platform was not found at the end of 60 seconds, the mouse was guided there by the experimenter, where it remained on the platform for ten seconds before being moved to a rest block for one minute (Intertrial interval of 70 sec). Swim path data were obtained using a computerized tracking system (Datawave) and included escape distance (cm), latency to reach the platform (sec) and swim speed. Errors were recorded by the experimenter and were counted when the mouse's hind legs entered an arm without reaching the platform or if the mouse stayed in one arm for >15 sec without reaching the platform. Data averaged from the match trials were used in analyses.

Testing: Win-shift task—This four day task consisted of twelve trials per day, with goal arm location being randomly chosen without same day repeats and changed before sample trials 1, 5, and 9. Intertrial intervals remained constant at 70sec in between trials, whether or not there was a platform location change. Averaged data from trials 2-4, 6-8, and 10-12 (the match trials) were used for analysis. Data were log-transformed in order to ensure Gaussian distribution for statistical analysis.

Statistics

All data are presented in the figures as mean values ± SEM. Statistical tests were performed with GraphPad Prism software. Unpaired student's t-tests were used to compare neuron, spine, synapse and immunofluorescent puncta densities; puncta area and dendritic arbor length. The immunoblot data shown in Fig. 1 were analyzed with a two-tailed, paired t-test. Developmental western blot data of Fig. 2 were analyzed using a one-way ANOVA and Bonferroni post-hoc tests. Scholl data were analyzed by a two-way mixed-model repeated-measures ANOVA with genotype as a between-groups factor and radial distance from soma (in 30 μm increments) as a within-group factor. Differences at individual distances in the Sholl analysis were determined with Bonferroni post-hoc tests. Performance on behavioral tasks was analyzed using a two-way repeated-measures ANOVA or Student's t-tests, where appropriate. For all tests, $\alpha = 0.05$.

Results

Timecourse of conditional N-cadherin deletion

In order to delete N-cadherin from excitatory neurons of the hippocampus, we crossed a mouse line expressing floxed N-cadherin with another line expressing Cre recombinase driven by the αCaMKII promoter as we reported previously (Bozdagi et al. 2010). As expected from the onset of expression of Cre recombinase (Tsien et al. 1996; Fukaya et al. 2003; Sonner et al. 2005; Gould et al. 2008), N-cadherin levels in hippocampal lysates taken from conditional knockout (cKO) mice (Ncad $^{flox/flox}$; Cre$^{-/+}$) were comparable to floxed

control mice ($Ncad^{flox/flox}$; $Cre^{-/-}$) at two postnatal weeks, but then declined significantly thereafter (Fig. 2A, $p<0.01$). In sections from hippocampus, N-cadherin immunofluorescence, which is typically punctate reflecting localization at synapses, was also largely eliminated throughout hippocampus in dentate gyrus (DG) and CA3 as well as in CA1 in the cKO mice (Fig. 2B, E) (Bozdagi et al. 2010). The residual N-cadherin was expressed by astrocytes, endothelial cells and GABA neurons (Bozdagi et al. 2010), none of which express αCaMKII-Cre and would therefore not be affected by the mutation.

In cultured cell lines, N-cadherin protects ß-catenin from degradation through binding (Sadot et al. 1998). We therefore analyzed whether conditional loss of N-cadherin in neurons would affect levels of ß-catenin. We found that at two postnatal weeks, prior to onset of N-cadherin ablation, there were no differences between genotypes in hippocampal ß-catenin levels, but by 24 weeks, ß-catenin levels were significantly lower in N-cadherin cKO mice in comparison with floxed controls (Fig. 2C, $p<0.05$). Quantitative immunolocalization verified the western blot analysis and revealed significantly diminished density of ß-catenin immunolabeled puncta in CA1 (Fig. 2D, F; $p < 0.01$) and DG (Fig. 2D, F; $p < 0.05$). In CA3, the density of ß-catenin puncta was on average lower in comparison with floxed controls, but this difference was not statistically significant (Fig. 2D, F; $p=0.33$). Together, these converging data demonstrate both the late postnatal onset of N-cadherin ablation and a correlated reduction in ß-catenin levels in hippocampus of cKO mice.

Effects of conditional deletion on hippocampal neuronal structure

The N-cadherin/ß-catenin complex has been implicated in synaptogenesis and morphogenesis of dendritic arbors and spines (Yu and Malenka 2003; Okuda et al. 2007; Hirano and Takeichi 2012). We therefore asked whether N-cadherin was important for the maintenance of dendritic arbors and synaptic architecture in adulthood. Reconstructions of CA1 neurons that had been intracellularly filled with Lucifer Yellow showed no differences in pyramidal cell dendritic branching (Fig. 3A, B; $p > 0.1$) or total dendritic arbor length (Fig. 3C, $p > 0.2$). Additionally stereological analysis of sections using electron microscopy showed no differences in CA1 neuron density (Fig. 3D-F, $p > 0.8$) nor in numbers of excitatory synapses-per-neuron (Fig. 3G-I, $p > 0.9$) between cKO and floxed control mice. Dentate gyrus incorporates new neurons throughout life and might be expected to be more vulnerable to the loss of N-cadherin, but comparisons of dendritic spine density and morphology showed no evidence for differences between genotypes in the overall density of spines nor in the distribution of morphological subtypes of spines (thin, stubby, mushroom) in DG, CA3 or CA1 (Fig. 4). Together, these data demonstrate that in maturity, hippocampal synaptic circuitry and architecture are maintained normally in the absence of N-cadherin, unlike during early development.

Altered molecular composition of synapse in the absence of N-cadherin

N-cadherin is an integral component of a macromolecular complex of synaptic proteins (Husi et al. 2000). Thus, N-cadherin ablation could alter the level or localization of molecules within or near synapses that are unaltered in number or morphology. To test this idea, we immunolabeled the predominant glutamate receptor subunits found in adult CA1 synapses: GluA1, GluA2 and GluN1. Consistent with previous immunolocalization studies,

the distribution of each of these GluR markers was predominantly clustered, representing both synaptic and non-synaptic pools (Huntley et al. 1994; Baude et al. 1995; Fritschy et al. 1998; Rubio and Wenthold 1999; Petralia et al. 2010). We found that GluA1-immunopositive puncta were significantly decreased in density and size in all subfields of the hippocampus in the cKO mice compared to floxed controls (Fig. 5A-C). In contrast, there were no changes in density or size of puncta immunoreactive for GluA2 (Fig. 5D-F) or GluN1 (Fig. 5G-H) in any subfield. We did not attempt to examine co-distribution with presynaptic markers as an index of synaptic localization because antibodies penetrate thick-tissue sections to different depths, often yielding false negatives as demonstrated in previous studies using similar approaches (Piekut and Casey 1983; Huntley and Benson 1999; Brunig et al. 2002a; Stevens et al. 2007). Instead, we used Western blot analyses of synaptoneurosomes prepared from whole-hippocampal lysates to confirm a significantly diminished level of synaptic GluA1 (Fig. 6A, C), with no changes in levels of GluA2 (Fig. 6A,C), GluN1 (Fig. 6A, C) and GluN2B (Fig. 6A, C). Taking both anatomical and biochemical approaches together, the data suggest that levels of GluA1 are diminished in the absence of N-cadherin, and at least some of this represents the synaptic/perisynaptic pool.

GluA1 is dynamically positioned and maintained at the synapse by the scaffolding protein PSD95 (Schnell et al. 2002; Ehrlich and Malinow 2004) while GluA2 is positioned similarly at the synapse by the scaffolding protein S-SCAM/MAGI-2 (Danielson et al. 2012). We therefore tested whether the loss of GluA1 and the preservation of GluA2 reflected similar alterations in levels of their respective scaffolding proteins. In hippocampal sections from cKO mice immunolabeled for PSD95, a marker that is almost exclusively postsynaptically concentrated (Sans et al. 2000; Marrs et al. 2001; Chen X et al. 2011; MacGillavry et al. 2013), we found a significantly diminished density of PSD95-labeled puncta in all subfields in comparison with floxed controls (Fig. 5J, K) without changes in the size of the remaining puncta (Fig. 5L). The lower density of PSD95 puncta in the cKO hippocampus was matched by significantly decreased levels of synaptic PSD95 determined by immunoblot of synaptoneurosomes (Fig. 6B, C). In contrast, by similar methods, we found no significant differences between cKO and control mice in levels of synaptic S-SCAM/MAGI-2 (Fig. 6B, C).

In contrast to changes in levels and localization of GluA1 and PSD95, neither the levels nor the localization of presynaptic vesicle protein markers differed between cKO and floxed mice. Sections immunolabeled for both vesicular glutamate transporters 1 and 2 (vGluts1 and 2; Fig. 7A-C), which cluster at nearly all excitatory presynaptic terminals in hippocampus (Kaneko et al. 2002; Fremeau et al. 2004; Herzog et al. 2006), and immunoblots for synaptophysin, an integral synaptic vesicle protein (Navone et al. 1986) (Fig. 7D) were similar across genotypes. These observations are consistent with the previous demonstration that the paired-pulse ratio, a measure of presynaptic function, is unaltered at CA3-CA1 synapses in adult N-cadherin cKO mice (Bozdagi et al. 2010). Taken together, conditional ablation of N-cadherin alters the level and localization of a subset of signaling and scaffolding proteins on the postsynaptic side of glutamatergic excitatory synapses.

Compensatory alterations in GABAergic inhibitory circuitry

PSD95 knockdown in cultured hippocampal neurons increases the density of GABAergic innervation (Graf et al. 2004; Prange et al. 2004; Levinson et al. 2005; Levinson et al. 2010). If similar effects occur in the adult brain, then the reduced levels of PSD95 in the N-cadherin cKO mice should also increase GABAergic circuitry in the hippocampus. We tested this idea first by evaluating whether GABAergic inhibition was altered functionally in the hippocampus of cKO mice. This was accomplished using a standard protocol of measuring the severity of behavioral seizures in response to administration of the anticonvulsant kainic acid or saline (vehicle) to adult male cKO or wildtype mice. The rationale behind this approach is that levels of GABAergic inhibition can regulate seizure severity (Ben-Ari and Cossart 2000), thus differences between genotypes in seizure severity could indicate that GABAergic circuits are altered in the cKO mice. We administered kainic acid or saline and then scored resulting seizure activity over time according to a 6-point scale, where 0 = no seizure activity and 6 = whole-body tonic-clonic convulsions (McKhann et al. 2003) (see Materials and Methods). No animal displayed any seizure activity prior to drug administration or following injection of saline alone (Fig. 8A). However, as predicted, the cKO mice displayed a significantly lower seizure severity profile in comparison with controls following kainic acid administration (Fig. 8H; cKO mice: 1.91 ± 0.13 vs control mice: 3.94 ± 0.15; $p < 0.0002$, unpaired Student's t-test). These data are consistent with the idea that functional GABAergic inhibition is increased in the cKO mice.

We next analyzed a potential anatomical basis for such changes in seizure severity by examining the density of pre- and postsynaptic GABA markers in CA1 in immunolabeled hippocampal sections from adult cKO and floxed mice. An antibody to the 65kD isoform of glutamic acid decarboxylase (GAD65) marked presynaptic GABAergic boutons; an antibody to gephyrin, a $GABA_A$ receptor anchoring molecule, marked postsynaptic GABAergic sites. Previous localization studies have shown that at GABA synapses, gephyrin forms multiple, smaller clusters in comparison with GAD65-labeled boutons (Brunig et al. 2002b; Bozdagi *et al.* 2004; Tyagarajan and Fritschy 2014), consistent with our observations in both cKO and floxed mice (Fig. 8B, C, E, F). Both GAD65 (Fig. 8B-D) and gephyrin (Fig. 8E-G) puncta densities were increased in the cKO mice compared to floxed controls, without any detectable changes in puncta size (Fig. 8D, G). We next examined overall hippocampal levels of GAD65, gephryin and VGAT by immunoblot, and found no overt differences between genotypes in levels of these proteins (Fig. 8H). Taken together, these data suggest that functional GABA inhibition is increased in cKO mice by a redistribution of molecules on both pre- and postsynaptic sides of the synapse.

Cognitive deficits in the absence of N-cadherin

The molecular changes to hippocampal synapses described above together with previously reported deficits in persistence of LTP at CA1 synapses (Bozdagi et al. 2010) suggest that hippocampal dependent cognition should be impaired in the cKO mice. Indeed, spatial learning and memory, but not other behavior abilities, were impaired in the cKO (n=13) compared to the floxed control (n=11) mice. The two groups had similar general health, spontaneous activity, elicited reflexes, sensory and motor functions, grip strength, and performance on a rotarod (the SHIRPA protocol (Rogers et al. 1997)), as well as similar

locomotor activity and anxiety measured in an open field test (data not shown). Performance in a six-arm radial water maze, however, varied with cognitive demand and hippocampal dependent memory function.

A water maze had six arms radiating from a central open area (Fig. 9A,B). In each task, the mouse was placed at the end of one alley and could escape the water by swimming to the end of another alley and climbing onto a platform. Performance was measured by the number of incorrect arm entries, as well as the duration and distance of each swim. Both cKO and floxed control mice learned rapidly to approach the platform when it was visible, verifying that sensory, perceptual, motivational and motor abilities were intact in the cKO mice (Fletcher et al. 2007; Shirvalkar et al. 2010). This cue-approach task does not require spatial memory or hippocampal function (Morris et al. 1986; Fletcher et al. 2006) (Fig. 9C). The cKO mice were impaired, however, in a matching-to-place task that required the animals to learn and remember hidden platform locations. In one task, the platform was kept in the same location for each day's testing session, but changed from one day to the next. Therefore, in the first, sample trial of the day, the mouse explored each arm and found the platform by trial and error. During the next seven match trials, the mouse was placed in a different start arm and could return directly to the platform by remembering its location. Both groups learned the general rules of the matching task at similar rates, reaching the platform in <12 seconds in four consecutive trials within four training days (Fig. 9C). Both groups also performed similarly during the sample trials, when the mice had to explore the maze to find the platform and memory could not guide performance (errors, escape latencies, and swim distances were equivalent in both genotypes, ($t(22)$: errors = 1.41, $p>0.17$; latency = 1.38, $p=0.18$ and distance = 1.70, $p=0.10$).

During matching trials, however, the cKO mice revealed deficits in both spatial learning and the persistence of spatial memory. Floxed control mice swam more directly to the escape platform and made fewer errors than the cKO mice (Fig. 9A,B,D,E; $p < 0.05$). The floxed mice also demonstrated memory for the previous day's platform position by returning to that location the next day in "perseverative errors". The proportion of these entries into the previous day's goal was significantly higher in the floxed control than the cKO mice (Fig. 9F, $p < 0.05$). Hence, the floxed mice made fewer errors than the cKO mice overall, and those errors suggested memory for the previous day's platform location. The cKO mice made more errors overall, and the pattern of errors revealed no memory for the previous day's platform location.

To further test memory demand and cognitive flexibility, we increased proactive interference by giving the mice three matching-to-place tests each day. For each block of four trials the platform was kept in the same place, the first trial was a sample, and the next three were matches. The platform was moved after each block, and the mice were tested on three blocks each day. The cKO and floxed control mice performed similarly during the sample trials ($t(22)$: errors=0.18, $p=0.74$; distance=0.14, $p=0.77$; latency=0.09, $p=0.79$), showing intact exploratory behavior. Overall across all matching trials, the cKO mice were impaired, with longer swim paths despite showing no difference in swim speed (cKO: 309.0 ± 29.6 cm; floxed: 228.3 ± 18.1 cm, $F(1,22)$: distance=5.601, $p<0.05$; speed=0.001, $p=0.97$) . While errors and latencies were not significantly different when averaged across all days ($F(1,22)$:

errors=3.97, p=0.06; latency=3.25, p=0.09), there were significant differences in performance between genotypes as time progressed. The control mice adapted to the high interference condition, and made fewer errors at the end of testing then at the beginning, whereas the cKO mice made more errors and did not improve (Fig. 9G, repeated measures ANOVA, first vs last testing days, F(1,22): genotype = 3.34, p = 0.08; days = 16.2, p < 0.01; genotype x day = 5.12, p < 0.05). Similarly, by the last two days of testing, significant differences in performance were evident between genotypes in the latency (F(1,22): genotype=3.07, p=0.09; days=6.28, p<0.05; genotype x day=2.59, p=0.12) and swim paths (F(1,22): genotype=5.21, p<0.05; days=9.03, p<0.01; genotype x day=1.94, p=0.18) (Fig. 9H, I).

Together, the data suggest that while both genotypes learned task rules and were motivated to escape to the platform, the cKO mice learned slower and remembered less than the floxed control mice. When the platform location moved once a day, the cKO mice made more spatial memory errors, and the errors were not influenced by memory for the previous day's platform location, in contrast to the floxed control mice. When the platform moved several times a day, the cKO mice adapted poorly to the new contingencies and did not learn to return efficiently to the most recent platform location.

Discussion

By using a conditional genetic ablation strategy in mice that eliminates N-cadherin and reduces levels of β-catenin at excitatory forebrain synapses starting in late postnatal life, we show that in maturity, N-cadherin/β-catenin take on new and selective roles in regulating levels and localization of postsynaptic glutamate receptor subunits and their associated scaffolding molecules. We found that GluA1 and PSD95 levels and density of immunoreactive puncta were significantly diminished across all subfields of the hippocampus, while in contrast, levels and localization of GluA2, its postsynaptic scaffold S-SCAM/MAGI-2 and NMDAR subunits GluN1 and GluN2B were unchanged. Surprisingly, the cKO mice also displayed a significantly greater density of pre- and postsynaptic GABAergic inhibitory synapse markers in CA1 and a higher threshold for kainic acid-induced seizures. Together, this suggests that there is a compensatory increase in functional inhibition in the absence of N-cadherin. Collectively, such molecular alterations in both excitatory and inhibitory circuits within the hippocampus likely contribute to deficient maintenance of hippocampal LTP (Bozdagi et al. 2010) as well as impaired hippocampal-dependent cognitive function, as we found that adult cKO mice displayed profound deficits in memory for spatial episodes.

A selective role for the N-cadherin/β-catenin complex in modulating the activity-dependent regulated pathway of AMPAR subunit trafficking in vivo

We demonstrated previously that adult N-cadherin cKO mice exhibit significant impairment in persistence, but not induction, of LTP and accompanying spine enlargement at CA1 synapses (Bozdagi et al. 2010). Our observations here suggest a plausible basis for such abnormal synaptic plasticity. At adult hippocampal synapses, AMPARs consist predominantly of hetero-oligomers comprising either GluA1/GluA2 subunits or GluA2/

GluA3 subunits (Wenthold et al. 1996). PSD95 contributes to membrane-surface delivery of GluA1 as part of a regulated, activity-dependent pathway (Passafaro et al. 2001; Schnell et al. 2002; Stein et al. 2003; Ehlers et al. 2007; Yudowski et al. 2007; Yang et al. 2008; Opazo and Choquet 2011). Although not universally agreed upon (Granger et al. 2013), many studies indicate that such synaptic delivery of GluA1 via PSD95 is required for persistence of LTP and spine enlargement (Shi et al. 1999; Ehrlich and Malinow 2004; Park et al. 2004; Kopec et al. 2006; Kopec et al. 2007; Yang et al. 2008). Thus, the failure of LTP and spine enlargement to persist at cKO synapses is likely a direct reflection of diminished levels of GluA1 and PSD95; normal *induction* of both forms of synaptic plasticity, which requires NMDARs (Yang et al. 2008), is consistent with unaltered levels and localization of GluN1 and GluN2B. In cell culture, N-cadherin can bind directly to GluA1 *in cis* through ectodomain interactions, while a dominant-negative form of N-cadherin reduces surface GluA1 levels (Nuriya and Huganir 2006). Thus, *in vivo*, levels of GluA1 and/or PSD95 may be insufficient for proper extrasynaptic delivery and/or incorporation into the synapse during LTP. Alternatively, residual levels of these molecules may be sufficient for proper delivery, but the lack of N-cadherin impairs synaptic insertion or trapping of GluA1. In any event, this scenario implies that one primary function of the N-cadherin/β-catenin complex at adult synapses is to translate activity patterns into appropriate molecular signaling cascades that support persistent synaptic plasticity. How this occurs mechanistically remains to be investigated, but relevant signals could be generated by any number of dynamic changes that N-cadherin or β-catenin undergo in response to appropriate patterns of synaptic activity, including changes in conformation, localization, dimerization and downstream signaling cascades (Tang et al. 1998; Bozdagi et al. 2000; Tanaka et al. 2000; Murase et al. 2002; Tai et al. 2007; Yasuda et al. 2007).

Trapping of GluA1 at the synapse might also be expected to fail because of reduced levels of PSD95 “slots”, which are thought to anchor AMPAR-TARP (transmembrane AMPAR regulatory protein) complexes to the synaptic membrane during LTP (Opazo et al. 2012). Alternatively, the diminished level of GluA1 may be secondary to the diminished level of PSD95, since PSD95 knockdown reduces surface levels of GluA1 (Nakagawa et al. 2004; Chen X et al. 2011). The loss of PSD95, in turn, could reflect diminished levels of β-catenin, as these molecules have been shown to interact biochemically in cultured chick retinal ganglion cells (Honjo et al. 2000).

In contrast to impaired persistence of LTP and spine plasticity at mutant CA1 synapses, properties of baseline synaptic neurotransmission in CA1 are unaltered in these adult cKO mice in comparison with controls (Bozdagi et al. 2010). GluA2 is delivered to synapses through a constitutive pathway (Shi et al. 2001; Malinow and Malenka 2002; Ehrlich and Malinow 2004) that requires interactions with S-SCAM/MAGI-2 for maintaining normal synaptic levels (Danielson et al. 2012). The present results suggest that the preserved levels of GluA2 and S-SCAM/MAGI-2 in the cKO mice are sufficient for maintaining normal properties of baseline synaptic transmission in part due to the sustained availability of S-SCAM/MAGI-2 in the cKO mice. This was unexpected in light of the diminished levels of β-catenin, as synaptic targeting of this scaffold depends on binding to β-catenin in developing neurons (Nishimura et al. 2002). Appropriate GluA2 localization may also be supported by binding interactions with other proteins, including GRIP (glutamate receptor

interacting protein), ABP (AMPAR binding protein), NSF (N-ethylamide-sensitive fusion protein), PICK1 (protein interacting with C-kinase-1) and β3-containing integrins (Malinow and Malenka 2002; Cingolani et al. 2008). GluA1, which is diminished in the cKO mice, likely does not normally contribute to basal AMPAR responses as there are no changes in baseline synaptic properties at CA1 synapses in GluA1 knockout mice (Zamanillo et al. 1999) nor in wildtype mice exposed to spermine, a polyamine that blocks GluA2-lacking AMPARs (Mainen et al. 1998). Taken together, the results here establish a molecular framework of predictable alterations in GluR function that can be tested by combined electrophysiological/pharmacological approaches in future studies.

Lack of presynaptic effects of N-cadherin deletion at mature excitatory synapses in vivo

Previous studies, principally in cultured neurons, have shown that knockdown of N-cadherin or β-catenin alters presynaptic vesicle accumulation and functional properties of release at excitatory synapses (Bamji et al. 2003; Bozdagi et al. 2004; Jungling et al. 2006; Sun et al. 2009; Stan et al. 2010; Sun and Bamji 2011; Pielarski et al. 2013). It was therefore surprising to find no overt evidence for changes in levels or localization of excitatory presynaptic molecular markers (present results) or indices of presynaptic functional properties (Bozdagi et al. 2010) at adult mutant synapses. Together, these observations support the idea that functions of the N-cadherin-catenin system evolve over time: at early stages of synapse formation, the transsynaptic N-cadherin/β-catenin linkage establishes presynaptic and postsynaptic structure and function coordinately, likely through collaborative interactions with other molecules such as Neuroligin (Nlg)-1 and S-SCAM/MAGI-2 (Stan et al. 2010). However, at more mature stages, N-cadherin functions predominantly postsynaptically, becoming dispensable for maintenance of excitatory presynaptic organization.

Compensatory changes in GABAergic circuitry

N-cadherin is not normally localized to mature hippocampal or neocortical GABAergic synapses (Benson and Tanaka 1998; Huntley and Benson 1999), but in the absence of N-cadherin, the density of markers of inhibitory synapses and seizure thresholds are increased. Somewhat surprisingly, however, we did not find by immunoblot that overall levels of several GABA synaptic molecular markers were elevated in the cKO mice. This could mean that in the absence of N-cadherin, GABA molecular markers are redistributed to new sites or accumulate at established sites at a level that allowed detection by immunolabeling. Alternatively, immunoblotting of whole-hippocampal tissue may not be sensitive enough to detect subtle changes in circuitry. Regardless of the precise mechanism, both functional and anatomical lines of evidence are consistent with increased inhibition in the conditional absence of N-cadherin. However, electrophysiological analysis of inhibitory synaptic function will be required in future studies to directly confirm this.

It is possible that the diminished levels of PSD95 resulting from N-cadherin deletion may have driven alterations in GABAergic circuitry through compensatory redistribution of Nlgs. PSD95 interacts with several Nlgs and coordinates different Nlg isoforms to specify excitatory and inhibitory synapses and to control proper balance of excitation and inhibition (Shipman et al. 2011). When levels of PSD95 are decreased in cultured neurons, synaptic

specificity of different Nlg isoforms is lost, resulting in greater numbers of GABA synapses and fewer numbers of excitatory synapses (Graf et al. 2004; Prange et al. 2004; Levinson et al. 2005; Levinson et al. 2010). Although it remains to be determined whether Nlg distribution is altered in the cKO mice, our data are consistent with this model in terms of an apparent increase in numbers of GABA synapses, but are inconsistent in that we did not find any differences in numbers of excitatory synapses. However, Nlg requires N-cadherin to regulate excitatory synapse number (Stan et al. 2010), thus in the absence of N-cadherin, PSD95/Nlg may exert their synaptogenic effects only on GABA synapses. Compensatory changes in levels of other cadherins may have also contributed. For example, in cultured neurons GABA synapse numbers are reduced following manipulations that reduce levels of E-cadherin (Fiederling et al. 2011), cadherin-11 or cadherin-13 (Paradis et al. 2007).

In the cKO mice, N-cadherin is deleted in principal neurons, but not in GABA neurons which lack αCaMKII-Cre (Tsien et al. 1996). Thus, excitatory synapses formed with GABA neurons in the cKO mice could, in theory, contain N-cadherin only on the postsynaptic side, leading to asymmetric transsynaptic interactions. Recent studies have shown that for excitatory synapses, such asymmetric postsynaptic localization of N-cadherin can alter synaptic number, function and molecular organization (Pielarski et al. 2013). Thus, speculatively, heterophilic interactions between N-cadherin in GABA neurons and other molecules, either *in cis* or *in trans*, could be driving compensatory changes in GABA circuits. For example, N-cadherin can interact with protocadherins (Pcdhs) (Weiner and Jontes 2013), and Pcdh-γC5 interacts directly with some subunits of the $GABA_A$ receptor, localizes to GABA synapses and can influence maintenance of GABA synapse numbers (Li et al. 2012).

Functional impact of conditional N-cadherin deletion

We found that adult cKO mice exhibited significant deficits in hippocampal-dependent memory for spatial episodes. In particular, while able to learn rules of the task during the sample trials to a degree similar to that of controls, they were subsequently incapable of persistent memory of relevant spatial information required for successful performance during match trials. Such cognitive inflexibility certainly must reflect, at least in part, the excitatory synaptic circuit-level deficits in the capacity for maintenance of LTP and spine plasticity (Bozdagi *et al.* 2010) as well as the selective molecular alterations in GluA1 and PSD95 discussed above. In contrast, GluA1 knockout mice lack LTP entirely (there is a failure of induction) and are deficient only in spatial working memory, but not spatial reference memory (Zamanillo et al. 1999; Reisel et al. 2002). Thus, deficits in synaptic plasticity or cognitive performance displayed by the N-cadherin cKO mice are unlike those displayed by GluA1 knockout mice, suggesting that additional circuit or molecular abnormalities must contribute to impaired information processing in the N-cadherin cKO mice. Fear-conditioning in mice elevates hippocampal levels of N-cadherin, and in turn is blocked in the presence of exogenous small-interferring peptides harboring the conserved HAV sequence found in classic cadherins and other cell-surface proteins (Schrick et al. 2007). Thus, it is possible that a failure of training-induced increases in N-cadherin levels in the cKO mice due to ablation of the gene contributed to deficient memory. The diminished levels of β-catenin may also have contributed, since conditional genetic ablation of β-catenin

in amygdala prevents consolidation, but not acquisition of fear memories (Maguschak and Ressler, 2008). It is also possible that the balance of excitation/inhibition (E/I) is disrupted in the cKO hippocampus, given the elevated number of GABA synapse markers and seizure threshold. When E/I balance is abnormal in other cortical areas, information processing is disturbed (Yizhar et al. 2011). Evaluation of the ratio of excitation-to-inhibition in the hippocampus of N-cadherin cKO mice will require detailed electrophysiological analyses, which is beyond the scope of the present study. In any event, cadherins have been linked genetically to susceptibility to autism and compulsive disorders (Ma et al. 2009; Wang et al. 2009; Dodman et al. 2010; Pagnamenta et al. 2010; Hussman et al. 2011). The results here provide a working model for future investigation of how cadherins contribute to human developmental brain disorders that reflect altered synaptic plasticity and function.

ACKNOWLEDGEMENTS

We thank Roxana Mesias, Steven Mortillo, Robert Rifkin and Becky Zhao for technical support, Dr. Prasad Shirvalkar for assistance with the water maze behavioral analyses, Dr. Greg Elder and Mr. Nathan Dorr for help with the SHIRPA protocol, and Dr. Alpha Yap for comments on the manuscript.

Grant Sponsor: National Institute of Mental Health grants MH075783 and F30MH088058; National Institute of Neurological Disorders and Stroke grants NS037731 and NS050634.

Literature Cited

Bamji SX, Shimazu K, Kimes N, Huelsken J, Birchmeier W, Lu B, Reichardt LF. Role of beta-catenin in synaptic vesicle localization and presynaptic assembly. Neuron. 2003; 40:719–731. [PubMed: 14622577]

Baude A, Nusser Z, Molnár E, McIlhinney RAJ, Somogyi P. High-resolution immunogold localization of AMPA type glutamate receptor subunits at synaptic and non-synaptic sites in rat hippocampus. Neurosci. 1995; 69:1031–1055.

Bekirov IH, Nagy V, Svoronos A, Huntley GW, Benson DL. Cadherin-8 and N-cadherin differentially regulate pre- and postsynaptic development of the hippocampal mossy fiber pathway. Hippocampus. 2008; 18:349–363. [PubMed: 18064706]

Ben-Ari Y, Cossart R. Kainate, a double agent that generates seizures: two decades of progress. Trends in Neurosci. 2000; 23:580–587.

Benson DL, Tanaka H. N-cadherin redistribution during synaptogenesis in hippocampal neurons. J Neurosci. 1998; 18:6892–6904. [PubMed: 9712659]

Bozdagi O, Shan W, Tanaka H, Benson DL, Huntley GW. Increasing numbers of synaptic puncta during late-phase LTP: N-cadherin is synthesized, recruited to synaptic sites, and required for potentiation. Neuron. 2000; 28:245–259. [PubMed: 11086998]

Bozdagi O, Valcin M, Poskanzer K, Tanaka H, Benson DL. Temporally distinct demands for classic cadherins in synapse formation and maturation. Mol Cell Neurosci. 2004; 27:509–521. [PubMed: 15555928]

Bozdagi O, Wang XB, Nikitczuk JS, Anderson TR, Bloss EB, Radice GL, Zhou Q, Benson DL, Huntley GW. Persistence of coordinated long-term potentiation and dendritic spine enlargement at mature hippocampal CA1 synapses requires N-cadherin. J Neurosci. 2010; 30:9984–9989. [PubMed: 20668183]

Brock JH, Elste A, Huntley GW. Distribution and injury-induced plasticity of cadherins in relationship to identified synaptic circuitry in adult rat spinal cord. J Neurosci. 2004; 24:8806–8817. [PubMed: 15470146]

Brunig I, Scotti E, Sidler C, Fritschy JM. Intact sorting, targeting, and clustering of gamma-aminobutyric acid A receptor subtypes in hippocampal neurons in vitro. J Comp Neurol. 2002a; 443:43–55. [PubMed: 11793346]

Brunig I, Suter A, Knuesel I, Luscher B, Fritschy JM. GABAergic terminals are required for postsynaptic clustering of dystrophin but not of GABA(A) receptors and gephyrin. J Neurosci. 2002b; 22:4805–4813. [PubMed: 12077177]

Chen DY, Stern SA, Garcia-Osta A, Saunier-Rebori B, Pollonini G, Bambah-Mukku D, Blitzer RD, Alberini CM. A critical role for IGF-II in memory consolidation and enhancement. Nature. 2011; 469:491–497. [PubMed: 21270887]

Chen X, Nelson CD, Li X, Winters CA, Azzam R, Sousa AA, Leapman RD, Gainer H, Sheng M, Reese TS. PSD-95 is required to sustain the molecular organization of the postsynaptic density. J Neurosci. 2011; 31:6329–6338. [PubMed: 21525273]

Cingolani LA, Thalhammer A, Yu LM, Catalano M, Ramos T, Colicos MA, Goda Y. Activity-dependent regulation of synaptic AMPA receptor composition and abundance by beta3 integrins. Neuron. 2008; 58:749–762. [PubMed: 18549786]

Coussen F, Normand E, Marchal C, Costet P, Choquet D, Lambert M, Mege RM, Mulle C. Recruitment of the kainate receptor subunit glutamate receptor 6 by cadherin/catenin complexes. J Neurosci. 2002; 22:6426–6436. [PubMed: 12151522]

Danielson E, Zhang N, Metallo J, Kaleka K, Shin SM, Gerges N, Lee SH. S-SCAM/MAGI-2 is an essential synaptic scaffolding molecule for the GluA2-containing maintenance pool of AMPA receptors. J Neurosci. 2012; 32:6967–6980. [PubMed: 22593065]

Dodman NH, Karlsson EK, Moon-Fanelli A, Galdzicka M, Perloski M, Shuster L, Lindblad-Toh K, Ginns EI. A canine chromosome 7 locus confers compulsive disorder susceptibility. Mol Psych. 2010; 15:8–10.

Ehlers MD, Heine M, Groc L, Lee MC, Choquet D. Diffusional trapping of GluR1 AMPA receptors by input-specific synaptic activity. Neuron. 2007; 54:447–460. [PubMed: 17481397]

Ehrlich I, Malinow R. Postsynaptic density 95 controls AMPA receptor incorporation during long-term potentiation and experience-driven synaptic plasticity. J Neurosci. 2004; 24:916–927. [PubMed: 14749436]

Elste AM, Benson DL. Structural basis for developmentally regulated changes in cadherin function at synapses. J Comp Neurol. 2006; 495:324–335. [PubMed: 16440298]

Fannon AM, Colman DR. A model for central synaptic junctional complex formation based on the differential adhesive specificities of the cadherins. Neuron. 1996; 17:423–434. [PubMed: 8816706]

Fiederling A, Ewert R, Andreyeva A, Jungling K, Gottmann K. E-cadherin is required at GABAergic synapses in cultured cortical neurons. Neurosci Letts. 2011; 501:167–172. [PubMed: 21782891]

Fletcher BR, Baxter MG, Guzowski JF, Shapiro ML, Rapp PR. Selective cholinergic depletion of the hippocampus spares both behaviorally induced Arc transcription and spatial learning and memory. Hippocampus. 2007; 17:227–234. [PubMed: 17286278]

Fletcher BR, Calhoun ME, Rapp PR, Shapiro ML. Fornix lesions decouple the induction of hippocampal arc transcription from behavior but not plasticity. J Neurosci. 2006; 26:1507–1515. [PubMed: 16452674]

Fremeau RT Jr. Kam K, Qureshi T, Johnson J, Copenhagen DR, Storm-Mathisen J, Chaudhry FA, Nicoll RA, Edwards RH. Vesicular glutamate transporters 1 and 2 target to functionally distinct synaptic release sites. Science. 2004; 304:1815–1819. [PubMed: 15118123]

Fritschy JM, Weinmann O, Wenzel A, Benke D. Synapse-specific localization of NMDA and GABA(A) receptor subunits revealed by antigen-retrieval immunohistochemistry. J Comp Neurol. 1998; 390:194–210. [PubMed: 9453664]

Fukaya M, Kato A, Lovett C, Tonegawa S, Watanabe M. Retention of NMDA receptor NR2 subunits in the lumen of endoplasmic reticulum in targeted NR1 knockout mice. Proc Natl Acad Sci USA. 2003; 100:4855–4860. [PubMed: 12676993]

Geinisman Y, Gundersen HJ, van der Zee E, West MJ. Unbiased stereological estimation of the total number of synapses in a brain region. J Neurocytol. 1996; 25:805–819. [PubMed: 9023726]

Gould TD, O'Donnell KC, Picchini AM, Dow ER, Chen G, Manji HK. Generation and behavioral characterization of beta-catenin forebrain-specific conditional knock-out mice. Behav Brain Res. 2008; 189:117–125. [PubMed: 18299155]

Graf ER, Zhang X, Jin SX, Linhoff MW, Craig AM. Neurexins induce differentiation of GABA and glutamate postsynaptic specializations via neuroligins. Cell. 2004; 119:1013–1026. [PubMed: 15620359]

Granger AJ, Shi Y, Lu W, Cerpas M, Nicoll RA. LTP requires a reserve pool of glutamate receptors independent of subunit type. Nature. 2013; 493:495–500. [PubMed: 23235828]

Herzog E, Takamori S, Jahn R, Brose N, Wojcik SM. Synaptic and vesicular co-localization of the glutamate transporters VGLUT1 and VGLUT2 in the mouse hippocampus. J Neurochem. 2006; 99:1011–1018. [PubMed: 16942593]

Hirano S, Takeichi M. Cadherins in brain morphogenesis and wiring. Physiol Rev. 2012; 92:597–634. [PubMed: 22535893]

Honjo Y, Nakagawa S, Takeichi M. Blockade of cadherin-6B activity perturbs the distribution of PSD-95 family proteins in retinal neurones. Genes Cells. 2000; 5:309–318. [PubMed: 10792468]

Huntley GW, Benson DL. Neural (N)-cadherin at developing thalamocortical synapses provides an adhesion mechanism for the formation of somatopically organized connections. J Comp Neurol. 1999; 407:453–471. [PubMed: 10235639]

Huntley GW, Vickers JC, Janssen W, Brose N, Heinemann SF, Morrison JH. Distribution and synaptic localization of immunocytochemically identified NMDA receptor subunit proteins in the sensory-motor cortex and visual cortices of monkey and human. J Neurosci. 1994; 14:3603–3619. [PubMed: 8207475]

Husi H, Ward MA, Choudhary JS, Blackstock WP, Grant SG. Proteomic analysis of NMDA receptor-adhesion protein signaling complexes. Nature Neurosci. 2000; 3:661–669. [PubMed: 10862698]

Hussman JP, Chung RH, Griswold AJ, Jaworski JM, Salyakina D, Ma D, Konidari I, Whitehead PL, Vance JM, Martin ER, Cuccaro ML, Gilbert JR, Haines JL, Pericak-Vance MA. A noise-reduction GWAS analysis implicates altered regulation of neurite outgrowth and guidance in autism. Mol Aut. 2011; 2:1.

Jungling K, Eulenburg V, Moore R, Kemler R, Lessmann V, Gottmann K. N-cadherin transsynaptically regulates short-term plasticity at glutamatergic synapses in embryonic stem cell-derived neurons. J Neurosci. 2006; 26:6968–6978. [PubMed: 16807326]

Kadowaki M, Nakamura S, Machon O, Krauss S, Radice GL, Takeichi M. N-cadherin mediates cortical organization in the mouse brain. Dev Biol. 2007; 304:22–33. [PubMed: 17222817]

Kaneko T, Fujiyama F, Hioki H. Immunohistochemical localization of candidates for vesicular glutamate transporters in the rat brain. J Comp Neurol. 2002; 444:39–62. [PubMed: 11835181]

Kleim JA, Luffnig E, Schwarz ER, Comery TA, Greenough WT. Synaptogenesis and FOS expression in the motor cortex of the adult rat after motor skill learning. J Neurosci. 1996; 16:4529–4535. [PubMed: 8699262]

Kopec CD, Li B, Wei W, Boehm J, Malinow R. Glutamate receptor exocytosis and spine enlargement during chemically induced long-term potentiation. J Neurosci. 2006; 26:2000–2009. [PubMed: 16481433]

Kopec CD, Real E, Kessels HW, Malinow R. GluR1 links structural and functional plasticity at excitatory synapses. J Neurosci. 2007; 27:13706–13718. [PubMed: 18077682]

Kostetskii I, Li J, Xiong Y, Zhou R, Ferrari VA, Patel VV, Molkentin JD, Radice GL. Induced deletion of the N-cadherin gene in the heart leads to dissolution of the intercalated disc structure. Circ Res. 2005; 96:346–354. [PubMed: 15662031]

Levinson JN, Chery N, Huang K, Wong TP, Gerrow K, Kang R, Prange O, Wang YT, El-Husseini A. Neuroligins mediate excitatory and inhibitory synapse formation: involvement of PSD-95 and neurexin-1beta in neuroligin-induced synaptic specificity. J Biol Chem. 2005; 280:17312–17319. [PubMed: 15723836]

Levinson JN, Li R, Kang R, Moukhles H, El-Husseini A, Bamji SX. Postsynaptic scaffolding molecules modulate the localization of neuroligins. Neurosci. 2010; 165:782–793.

Li Y, Xiao H, Chiou TT, Jin H, Bonhomme B, Miralles CP, Pinal N, Ali R, Chen WV, Maniatis T, De Blas AL. Molecular and functional interaction between protocadherin-gammaC5 and GABAA receptors. J Neurosci. 2012; 32:11780–11797. [PubMed: 22915120]

Ma D, Salyakina D, Jaworski JM, Konidari I, Whitehead PL, Andersen AN, Hoffman JD, Slifer SH, Hedges DJ, Cukier HN, Griswold AJ, McCauley JL, Beecham GW, Wright HH, Abramson RK,

Martin ER, Hussman JP, Gilbert JR, Cuccaro ML, Haines JL, Pericak-Vance MA. A genome-wide association study of autism reveals a common novel risk locus at 5p14.1. Ann Human Genetics. 2009; 73:263–273. [PubMed: 19456320]

MacGillavry HD, Song Y, Raghavachari S, Blanpied TA. Nanoscale scaffolding domains within the postsynaptic density concentrate synaptic AMPA receptors. Neuron. 2013; 78:615–622. [PubMed: 23719161]

Maguschak KA, Ressler KJ. Beta-catenin is required for memory consolidation. Nature Neurosci. 2008; 11:1319–1326. [PubMed: 18820693]

Mainen ZF, Jia Z, Roder J, Malinow R. Use-dependent AMPA receptor block in mice lacking GluR2 suggests postsynaptic site for LTP expression. Nature Neurosci. 1998; 1:579–586. [PubMed: 10196565]

Malinow R, Malenka RC. AMPA receptor trafficking and synaptic plasticity. Annu Rev Neurosci. 2002; 25:103–126. [PubMed: 12052905]

Marrs GS, Green SH, Dailey ME. Rapid formation and remodeling of postsynaptic densities in developing dendrites. Nature Neurosci. 2001; 4:1006–1013. [PubMed: 11574832]

McKhann GM, Wenzel HJ, Robbins CA, Sosunov AA, Schwartzkroin PA. Mouse strain differences in kainic acid sensitivity, seizure behavior, mortality, and hippocampal pathology. Neurosci. 2003; 122:551–561.

Mendez P, De Roo M, Poglia L, Klauser P, Muller D. N-cadherin mediates plasticity-induced long-term spine stabilization. J Cell Biol. 2010; 189:589–600. [PubMed: 20440002]

Morris RGM, Anderson E, Lynch GS, Baudry M. Selective impairment of learning and blockade of long-term potentiation by an *N*-methyl-D-aspartate receptor antagonist, AP5. Nature. 1986; 319:774–776. [PubMed: 2869411]

Murase S, Mosser E, Schuman EM. Depolarization drives beta-Catenin into neuronal spines promoting changes in synaptic structure and function. Neuron. 2002; 35:91–105. [PubMed: 12123611]

Nakagawa T, Futai K, Lashuel HA, Lo I, Okamoto K, Walz T, Hayashi Y, Sheng M. Quaternary structure, protein dynamics, and synaptic function of SAP97 controlled by L27 domain interactions. Neuron. 2004; 44:453–467. [PubMed: 15504326]

Navone F, Jahn R, di Gioia G, Stukenbrok H, Greengard P, De Camilli P. Protein p38: an integral membrane protein specific for small vesicles of neurons and neuroendocrine cells. J Cell Biol. 1986; 103:2511–2527. [PubMed: 3097029]

Nishimura W, Yao I, Iida J, Tanaka N, Hata Y. Interaction of synaptic scaffolding molecule and Beta -catenin. J Neurosci. 2002; 22:757–765. [PubMed: 11826105]

Nuriya M, Huganir RL. Regulation of AMPA receptor trafficking by N-cadherin. J Neurochem. 2006; 97:652–661. [PubMed: 16515543]

Okuda T, Yu LM, Cingolani LA, Kemler R, Goda Y. beta-Catenin regulates excitatory postsynaptic strength at hippocampal synapses. Proc Natl Acad Sci USA. 2007; 104:13479–13484. [PubMed: 17679699]

Opazo P, Choquet D. A three-step model for the synaptic recruitment of AMPA receptors. Mol Cell Neurosci. 2011; 46:1–8. [PubMed: 20817097]

Opazo P, Sainlos M, Choquet D. Regulation of AMPA receptor surface diffusion by PSD-95 slots. Curr Opin Neurobiol. 2012; 22:453–460. [PubMed: 22051694]

Pagnamenta AT, Khan H, Walker S, Gerrelli D, Wing K, Bonaglia MC, Giorda R, Berney T, Mani E, Molteni M, Pinto D, Le Couteur A, Hallmayer J, Sutcliffe JS, Szatmari P, Paterson AD, Scherer SW, Vieland VJ, Monaco AP. Rare familial 16q21 microdeletions under a linkage peak implicate cadherin 8 (CDH8) in susceptibility to autism and learning disability. J Med Genet. 2010; 48:48–54. [PubMed: 20972252]

Paradis S, Harrar DB, Lin Y, Koon AC, Hauser JL, Griffith EC, Zhu L, Brass LF, Chen C, Greenberg ME. An RNAi-based approach identifies molecules required for glutamatergic and GABAergic synapse development. Neuron. 2007; 53:217–232. [PubMed: 17224404]

Park M, Penick EC, Edwards JG, Kauer JA, Ehlers MD. Recycling endosomes supply AMPA receptors for LTP. Science. 2004; 305:1972–1975. [PubMed: 15448273]

Passafaro M, Piech V, Sheng M. Subunit-specific temporal and spatial patterns of AMPA receptor exocytosis in hippocampal neurons. Nature neuroscience. 2001; 4:917–926. [PubMed: 11528423]

Petralia RS, Wang YX, Hua F, Yi Z, Zhou A, Ge L, Stephenson FA, Wenthold RJ. Organization of NMDA receptors at extrasynaptic locations. Neurosci. 2010; 167:68–87.

Piekut DT, Casey SM. Penetration of immunoreagents in Vibratome-sectioned brain: a light and electron microscopic study. J Histochem Cytochem. 1983; 31:669–674. [PubMed: 6341457]

Pielarski KN, van Stegen B, Andreyeva A, Nieweg K, Jungling K, Redies C, Gottmann K. Asymmetric N-cadherin expression results in synapse dysfunction, synapse elimination, and axon retraction in cultured mouse neurons. PLoS One. 2013; 8:e54105. [PubMed: 23382872]

Poskanzer K, Needleman LA, Bozdagi O, Huntley GW. N-cadherin regulates ingrowth and laminar targeting of thalamocortical axons. J Neurosci. 2003; 23:2294–2305. [PubMed: 12657688]

Prange O, Wong TP, Gerrow K, Wang YT, El-Husseini A. A balance between excitatory and inhibitory synapses is controlled by PSD-95 and neuroligin. Proc Natl Acad Sci USA. 2004; 101:13915–13920. [PubMed: 15358863]

Racine RJ. Modification of seizure activity by electrical stimulation. II. Motor seizure. Electroencephalogr Clin Neurophysiol. 1972; 32:281–294. [PubMed: 4110397]

Radley JJ, Rocher AB, Miller M, Janssen WG, Liston C, Hof PR, McEwen BS, Morrison JH. Repeated stress induces dendritic spine loss in the rat medial prefrontal cortex. Cereb Cortex. 2006; 16:313–320. [PubMed: 15901656]

Reisel D, Bannerman DM, Schmitt WB, Deacon RM, Flint J, Borchardt T, Seeburg PH, Rawlins JN. Spatial memory dissociations in mice lacking GluR1. Nature Neurosci. 2002; 5:868–873. [PubMed: 12195431]

Rodriguez A, Ehlenberger DB, Hof PR, Wearne SL. Rayburst sampling, an algorithm for automated three-dimensional shape analysis from laser scanning microscopy images. Nat Protoc. 2006; 1:2152–2161. [PubMed: 17487207]

Rogers DC, Fisher EM, Brown SD, Peters J, Hunter AJ, Martin JE. Behavioral and functional analysis of mouse phenotype: SHIRPA, a proposed protocol for comprehensive phenotype assessment. Mamm Genome. 1997; 8:711–713. [PubMed: 9321461]

Rubio ME, Wenthold RJ. Differential distribution of intracellular glutamate receptors in dendrites. J Neurosci. 1999; 19:5549–5562. [PubMed: 10377362]

Sadot E, Simcha I, Shtutman M, Ben-Ze'ev A, Geiger B. Inhibition of beta-catenin-mediated transactivation by cadherin derivatives. Proc Natl Acad Sci USA. 1998; 95:15339–15344. [PubMed: 9860970]

Sans N, Petralia RS, Wang YX, Blahos J 2nd, Hell JW, Wenthold RJ. A developmental change in NMDA receptor-associated proteins at hippocampal synapses. J Neurosci. 2000; 20:1260–1271. [PubMed: 10648730]

Schnell E, Sizemore M, Karimzadegan S, Chen L, Bredt DS, Nicoll RA. Direct interactions between PSD-95 and stargazin control synaptic AMPA receptor number. Proc Natl Acad Sci USA. 2002; 99:13902–13907. [PubMed: 12359873]

Schrick C, Fischer A, Srivastava DP, Tronson NC, Penzes P, Radulovic J. N-cadherin regulates cytoskeletally associated IQGAP1/ERK signaling and memory formation. Neuron. 2007; 55:786–798. [PubMed: 17785185]

Shi S, Hayashi Y, Esteban JA, Malinow R. Subunit-specific rules governing AMPA receptor trafficking to synapses in hippocampal pyramidal neurons. Cell. 2001; 105:331–343. [PubMed: 11348590]

Shi SH, Hayashi Y, Petralia RS, Zaman SH, Wenthold RJ, Svoboda K, Malinow R. Rapid spine delivery and redistribution of AMPA receptors after synaptic NMDA receptor activation. Science. 1999; 284:1811–1816. [PubMed: 10364548]

Shipman SL, Schnell E, Hirai T, Chen BS, Roche KW, Nicoll RA. Functional dependence of neuroligin on a new non-PDZ intracellular domain. Nature Neurosci. 2011; 14:718–726. [PubMed: 21532576]

Shirvalkar PR, Rapp PR, Shapiro ML. Bidirectional changes to hippocampal theta-gamma comodulation predict memory for recent spatial episodes. Proc Natl Acad Sci USA. 2010; 107:7054–7059. [PubMed: 20351262]

Sonner JM, Cascio M, Xing Y, Fanselow MS, Kralic JE, Morrow AL, Korpi ER, Hardy S, Sloat B, Eger EI 2nd, Homanics GE. Alpha 1 subunit-containing GABA type A receptors in forebrain

contribute to the effect of inhaled anesthetics on conditioned fear. Mol Pharmacol. 2005; 68:61–68. [PubMed: 15833735]

Stan A, Pielarski KN, Brigadski T, Wittenmayer N, Fedorchenko O, Gohla A, Lessmann V, Dresbach T, Gottmann K. Essential cooperation of N-cadherin and neuroligin-1 in the transsynaptic control of vesicle accumulation. Proc Natl Acad Sci USA. 2010; 107:11116–11121. [PubMed: 20534458]

Stein V, House DR, Bredt DS, Nicoll RA. Postsynaptic density-95 mimics and occludes hippocampal long-term potentiation and enhances long-term depression. J Neurosci. 2003; 23:5503–5506. [PubMed: 12843250]

Stevens B, Allen NJ, Vazquez LE, Howell GR, Christopherson KS, Nouri N, Micheva KD, Mehalow AK, Huberman AD, Stafford B, Sher A, Litke AM, Lambris JD, Smith SJ, John SW, Barres BA. The classical complement cascade mediates CNS synapse elimination. Cell. 2007; 131:1164–1178. [PubMed: 18083105]

Sun Y, Aiga M, Yoshida E, Humbert PO, Bamji SX. Scribble interacts with beta-catenin to localize synaptic vesicles to synapses. Mol Biol Cell. 2009; 20:3390–3400. [PubMed: 19458197]

Sun Y, Bamji SX. beta-Pix modulates actin-mediated recruitment of synaptic vesicles to synapses. J Neurosci. 2011; 31:17123–17133. [PubMed: 22114281]

Tai CY, Kim SA, Schuman EM. Cadherins and synaptic plasticity. Curr Opin Cell Biol. 2008; 20:567–575. [PubMed: 18602471]

Tai CY, Mysore SP, Chiu C, Schuman EM. Activity-regulated N-cadherin endocytosis. Neuron. 2007; 54:771–785. [PubMed: 17553425]

Tanaka H, Shan W, Phillips GR, Arndt K, Bozdagi O, Shapiro L, Huntley GW, Benson DL, Colman DR. Molecular modification of N-cadherin in response to synaptic activity. Neuron. 2000; 25:93–107. [PubMed: 10707975]

Tang L, Hung CP, Schuman EM. A role for the cadherin family of cell adhesion molecules in hippocampal long-term potentiation. Neuron. 1998; 20:1165–1175. [PubMed: 9655504]

Togashi H, Abe K, Mizoguchi A, Takaoka K, Chisaka O, Takeichi M. Cadherin regulates dendritic spine morphogenesis. Neuron. 2002; 35:77–89. [PubMed: 12123610]

Tsien JZ, Chen DF, Gerber D, Tom C, Mercer EH, Anderson DJ, Mayford M, Kandel ER, Tonegawa S. Subregion- and cell type-restricted gene knockout in mouse brain. Cell. 1996; 87:1317–1326. [PubMed: 8980237]

Tyagarajan SK, Fritschy JM. Gephyrin: a master regulator of neuronal function? Nat Rev Neurosci. 2014; 15:141–156. [PubMed: 24552784]

Wang K, Zhang H, Ma D, Bucan M, Glessner JT, Abrahams BS, Salyakina D, Imielinski M, Bradfield JP, Sleiman PM, Kim CE, Hou C, Frackelton E, Chiavacci R, Takahashi N, Sakurai T, Rappaport E, Lajonchere CM, Munson J, Estes A, Korvatska O, Piven J, Sonnenblick LI, Alvarez Retuerto AI, Herman EI, Dong H, Hutman T, Sigman M, Ozonoff S, Klin A, Owley T, Sweeney JA, Brune CW, Cantor RM, Bernier R, Gilbert JR, Cuccaro ML, McMahon WM, Miller J, State MW, Wassink TH, Coon H, Levy SE, Schultz RT, Nurnberger JI, Haines JL, Sutcliffe JS, Cook EH, Minshew NJ, Buxbaum JD, Dawson G, Grant SF, Geschwind DH, Pericak-Vance MA, Schellenberg GD, Hakonarson H. Common genetic variants on 5p14.1 associate with autism spectrum disorders. Nature. 2009; 459:528–533. [PubMed: 19404256]

Wearne SL, Rodriguez A, Ehlenberger DB, Rocher AB, Henderson SC, Hof PR. New techniques for imaging, digitization and analysis of three-dimensional neural morphology on multiple scales. Neurosci. 2005; 136:661–680.

Weiner JA, Jontes JD. Protocadherins, not prototypical: a complex tale of their interactions, expression, and functions. Front Mol Neurosci. 2013; 6:4. [PubMed: 23515683]

Wenthold RJ, Petralia RS, Blahos J II, Niedzielski AS. Evidence for multiple AMPA receptor complexes in hippocampal CA1/CA2 neurons. J Neurosci. 1996; 16:1982–1989. [PubMed: 8604042]

Yamagata M, Herman JP, Sanes JR. Lamina-specific expression of adhesion molecules in developing chick optic tectum. J Neurosci. 1995; 15:4556–4571. [PubMed: 7790923]

Yamagata M, Sanes JR. Lamina-specific cues guide outgrowth and arborization of retinal axons in the optic tectum. Development. 1995; 121:189–200. [PubMed: 7867499]

Yang Y, Wang XB, Frerking M, Zhou Q. Delivery of AMPA receptors to perisynaptic sites precedes the full expression of long-term potentiation. Proc Natl Acad Sci USA. 2008; 105:11388–11393. [PubMed: 18682558]

Yang Y, Wang XB, Frerking M, Zhou Q. Spine expansion and stabilization associated with long-term potentiation. J Neurosci. 2008; 28:5740–5751. [PubMed: 18509035]

Yasuda S, Tanaka H, Sugiura H, Okamura K, Sakaguchi T, Tran U, Takemiya T, Mizoguchi A, Yagita Y, Sakurai T, De Robertis EM, Yamagata K. Activity-induced protocadherin arcadlin regulates dendritic spine number by triggering N-cadherin endocytosis via TAO2beta and p38 MAP kinases. Neuron. 2007; 56:456–471. [PubMed: 17988630]

Yizhar O, Fenno LE, Prigge M, Schneider F, Davidson TJ, O'Shea DJ, Sohal VS, Goshen I, Finkelstein J, Paz JT, Stehfest K, Fudim R, Ramakrishnan C, Huguenard JR, Hegemann P, Deisseroth K. Neocortical excitation/inhibition balance in information processing and social dysfunction. Nature. 2011; 477:171–178. [PubMed: 21796121]

Yu X, Malenka RC. Beta-catenin is critical for dendritic morphogenesis. Nature Neurosci. 2003; 6:1169–1177. [PubMed: 14528308]

Yudowski GA, Puthenveedu MA, Leonoudakis D, Panicker S, Thorn KS, Beattie EC, von Zastrow M. Real-time imaging of discrete exocytic events mediating surface delivery of AMPA receptors. J Neurosci. 2007; 27:11112–11121. [PubMed: 17928453]

Zamanillo D, Sprengel R, Hvalby O, Jensen V, Burnashev N, Rozov A, Kaiser KM, Koster HJ, Borchardt T, Worley P, Lubke J, Frotscher M, Kelly PH, Sommer B, Andersen P, Seeburg PH, Sakmann B. Importance of AMPA receptors for hippocampal synaptic plasticity but not for spatial learning. Science. 1999; 284:1805–1811. [PubMed: 10364547]

Zhang W, Benson DL. Stages of synapse development defined by dependence on F-actin. J Neurosci. 2001; 21:5169–5181. [PubMed: 11438592]

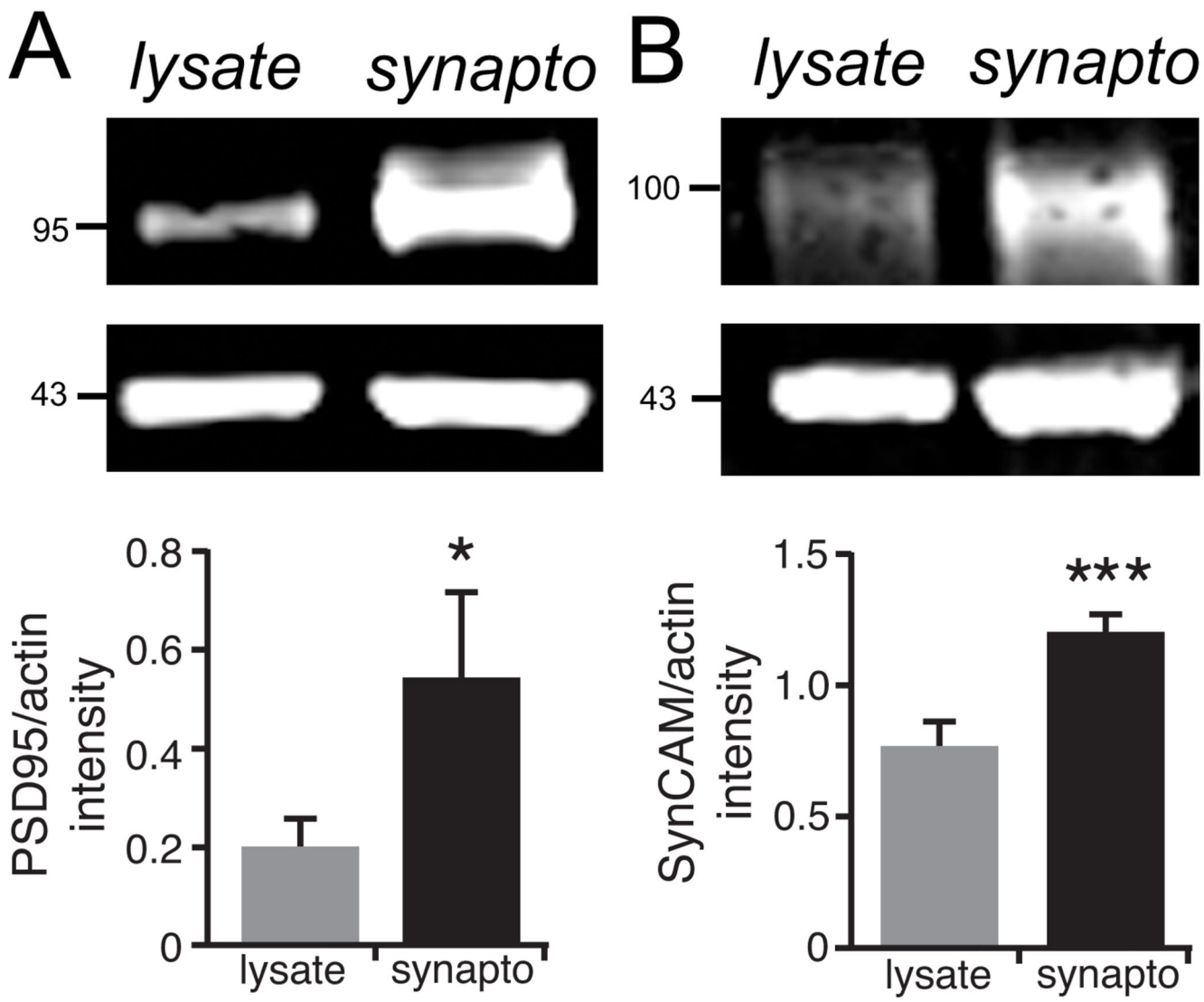

Fig 1. Enrichment of postsynaptic proteins in synaptoneurosomes

To verify the enrichment of synaptic proteins in the synaptoneurosome fraction, we prepared synaptoneurosomes (*synapto*) from whole-hippocampal lysates (*lysates*) taken from adult male wildtype mice (n=7-9) and blotted both fractions for PSD95 (clone 6G6-1C9) (**A**) or SynCAM (**B**), both of which are known to be enriched at glutamatergic hippocampal synapses. Actin was used as a loading control. The blots were visualized using a Li-Cor imaging system and quantified by expressing the ratio of the mean fluorescence intensity of PSD95 or SynCAM to that of their actin loading controls. As expected, both synaptic proteins were significantly enriched in the synaptoneurosome fraction. *$p<0.04$ or **$p<0.0002$; two-tailed paired t-test. Numbers (on left) indicate approximate positions of molecular mass markers (kDa).

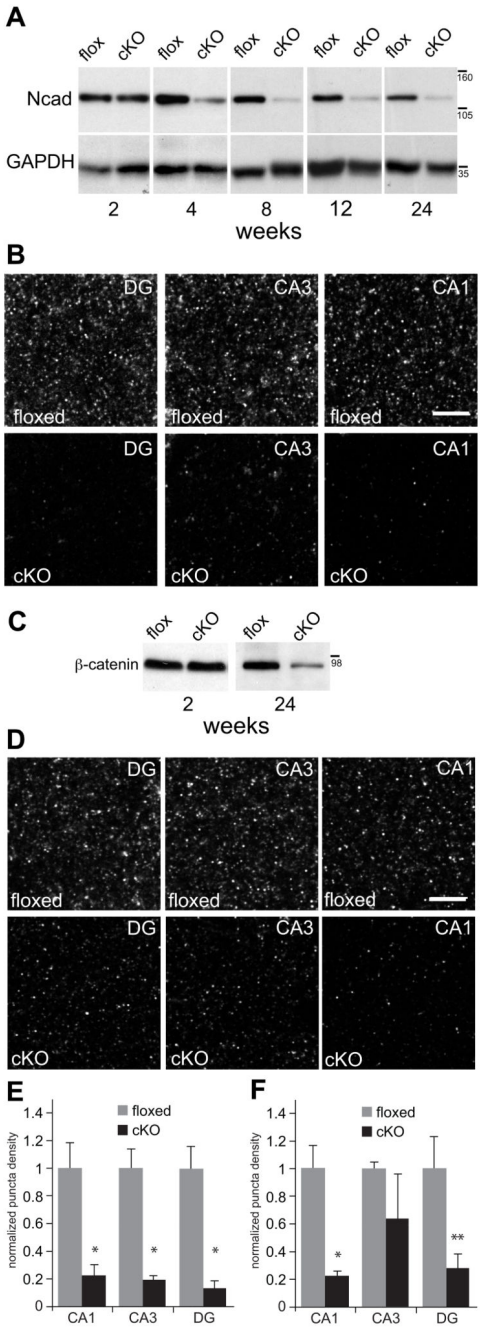

Fig. 2. N-cadherin is ablated and ß-catenin levels are diminished in N-cadherin cKO mice

A) Representative western blots of N-cadherin (Ncad) and GAPDH (used as a loading control) prepared from whole-hippocampal lysates at postnatal weeks indicated. There were no significant differences in N-cadherin levels across ages in the floxed control mice ($p > 0.6$, n=3 mice per genotype per age). At 2 postnatal weeks, N-cadherin levels in cKO mice were indistinguishable from those in control mice ($p > 0.5$). However, in comparison with age-matched floxed controls, N-cadherin levels in the cKO mice declined significantly by 4 postnatal weeks and remained significantly lower thereafter ($p < 0.01$). Statistical

comparisons across ages were assessed using one-way ANOVA. Numbers (on right) indicate approximate positions of molecular mass markers (kDa).

B) Representative patterns of N-cadherin immunolocalization in stratum radiatum (CA1 and CA3) or the molecular layer of the dentate gyrus (DG) of adult (5 mo-old) hippocampus. Bar = 5 μm.

C) Representative western blots of ß-catenin and GAPDH (used as a loading control) prepared from whole-hippocampal lysates at postnatal weeks indicated. There were no differences between genotypes in ß-catenin levels at 2 postnatal weeks ($p > 0.6$, n=3 mice per genotype per age), but by 24 weeks, ß-catenin levels were significantly diminished in the cKO hippocampus in comparison with floxed controls ($p < 0.05$). Statistical comparisons across ages were assessed using one-way ANOVA. Numbers (on right) indicate approximate positions of molecular mass markers (kDa).

D) Representative patterns of ß-catenin immunolocalization in stratum radiatum (CA1 and CA3) or the molecular layer of the dentate gyrus (DG) in adult (5 mo-old) hippocampus. Bar = 5 μm.

E) Quantitative analysis of N-cadherin puncta density confirmed a significant decrease in the cKO mice in comparison with floxed controls across all subfields (*$p < 0.01$, n=8 mice per genotype, unpaired Student's t-test).

F) Quantitative analysis of ß-catenin puncta density confirmed a significant decrease in the cKO mice in comparison with floxed controls in CA1 (*$p < 0.01$) and DG (**$p < 0.05$), but not in CA3 ($p=0.33$; n=4 per genotype, unpaired Student's t-test). In E and F, all quantitative values for each hippocampal subfield were normalized to floxed control values for that subfield.

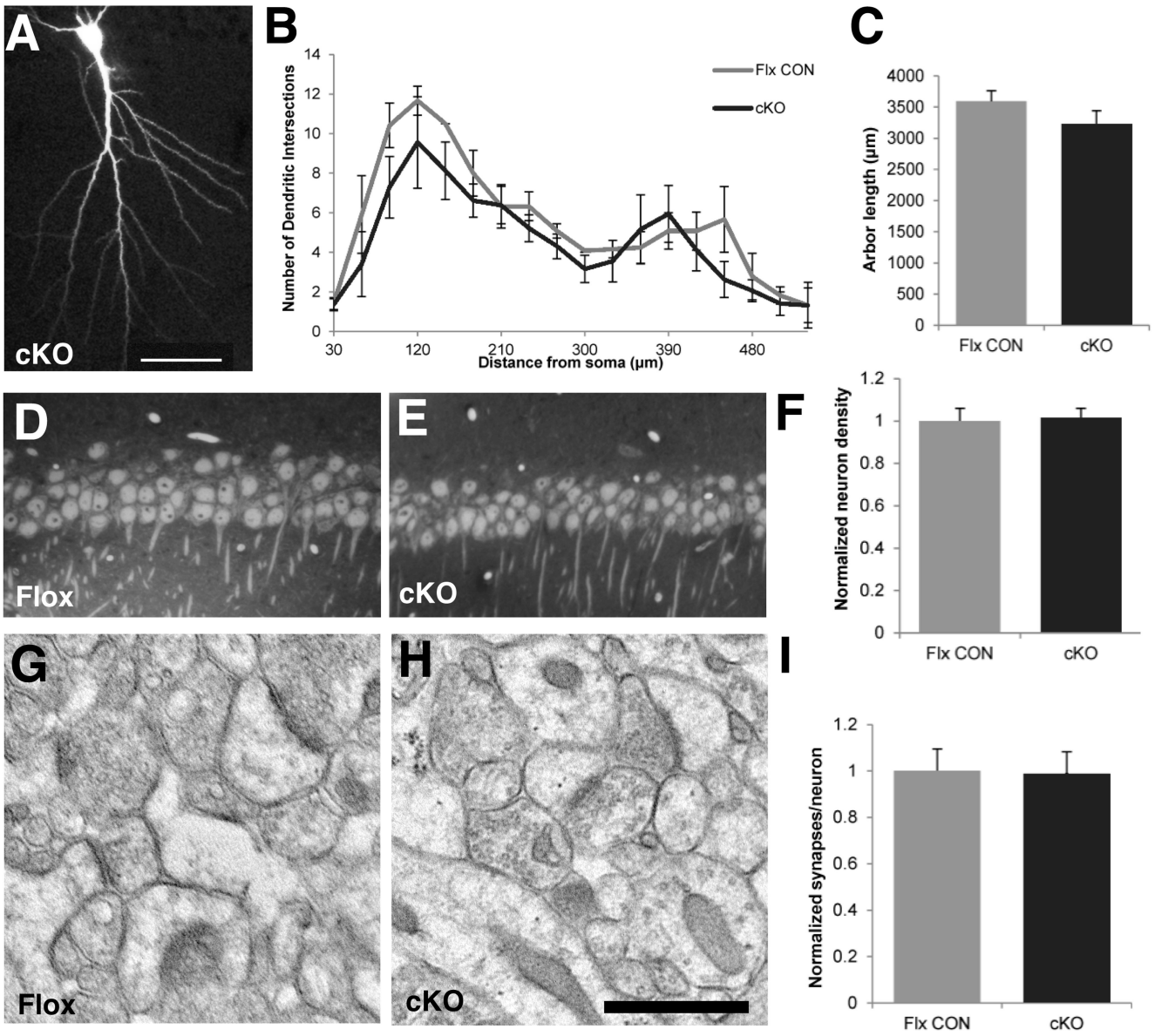

Fig. 3. N-cadherin is dispensible for maintaining dendritic architecture in adult hippocampal area CA1

A-C) Dendritic architecture is unchanged in cKO mice. Representative example (**A**) of a CA1 pyramidal cell taken from an adult cKO mouse and intracellularly filled with Lucifer Yellow. Bar = 50μm. Sholl analysis of CA1 pyramidal cell apical dendrites (**B**) showed no differences in branching between cKO mice and floxed control mice (n=3 mice per genotype; two-way repeated-measures ANOVA with genotype as a between-groups factor and radial distance from soma as a within-group factor). There were no differences between genotypes in total arbor length of CA1 pyramidal cell apical dendrites (**C**, p=0.27, unpaired Student's t-test). Dendrite analyses in B,C were based on 8 CA1 neurons from 3 adult male WT mice and 13 CA1 neurons from 4 male adult cKO mice.

D-F) Representative images of 1 μm-thick, plastic-embedded sections through CA1 pyramidal cell layer taken from a floxed control mouse (**D**) or a cKO mouse (**E**). Stereological analysis (**F**) revealed no significant differences in cell density between genotypes (n=3 mice per genotype, p=0.84, unpaired Student's t-test). All values were normalized to those of the floxed control mice.

G-H) Representative electron-micrographs through CA1 stratum radiatum taken from a floxed control mouse (**G**) or a cKO mouse (**H**). Bar=500 nm.

I) Stereological analysis revealed no significant differences in the number of synapses-per-neuron between cKO and floxed control mice (n=3 mice per genotype, p=0.94, unpaired Student's t-test). All values were normalized to those of the floxed control mice.

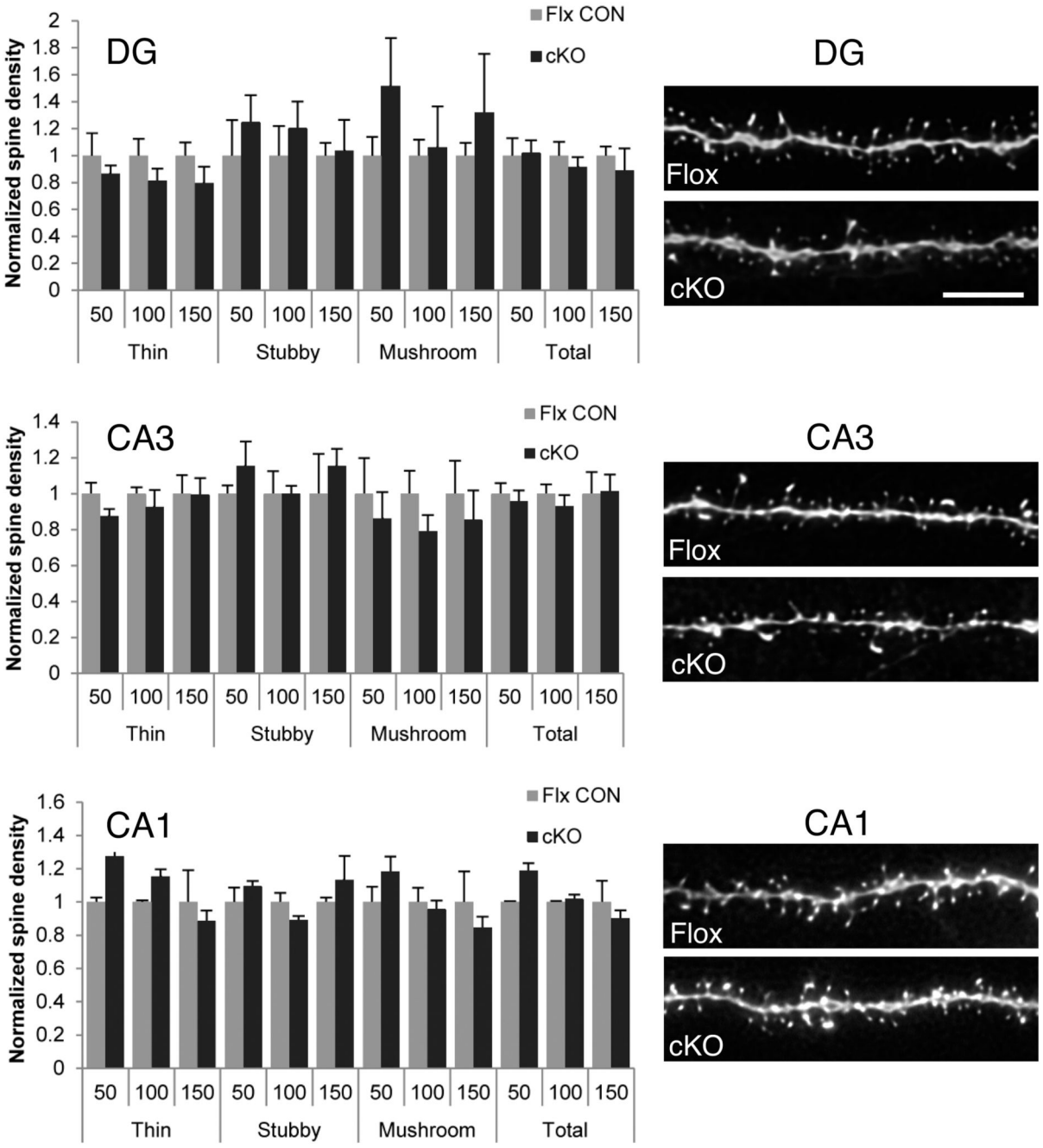

Fig. 4. Hippocampal spine density and morphology are unaltered in adult N-cadherin cKO mice

The graphs (left column) show quantification of density of total spines and of morphological subtypes (thin, stubby, mushroom) along apical dendritic segments located between 0-50 μm (50), 51-100 μm (100) or 101-150 μm (150) from the soma, from the indicated subfields and genotypes. This analysis showed no significant differences between genotypes in any subregion for either total spine density or for different morphological subtypes (thin, stubby, or mushroom) distributed over the different dendritic segments (unpaired Student's t-test. For each condition (region, dendritic segment, spine type), data are normalized to the floxed

control values for that condition). In the right column are representative confocal images of apical dendritic segments from intracellularly-filled neurons from the corresponding hippocampal subregions indicated. The material was taken from floxed control mice (flox, top image in each pair) or cKO mice (cKO, bottom image in each pair). Bar = 5μm.

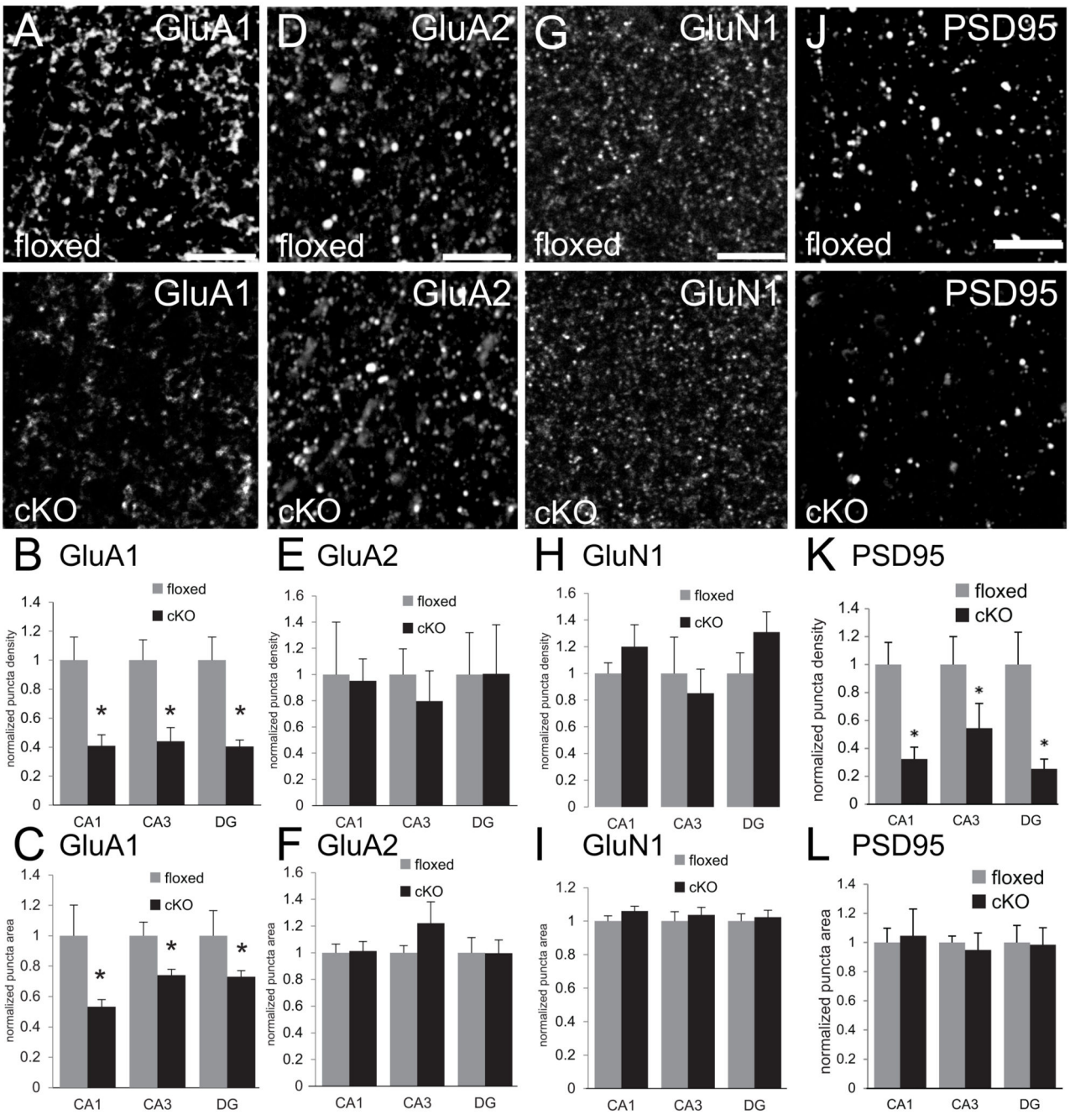

Fig. 5. Diminished density of GluA1 and PSD95 immunolabeled puncta in adult hippocampus of N-cadherin cKO mice

(**A,D,G,J**) Representative confocal microscope images of sections through stratum radiatum of CA1 of adult floxed control mice (top row) or cKO mice (bottom row) immunofluorescently labeled for AMPAR subunits GluA1 (**A**), GluA2 (**D**), NMDAR subunit GluN1 (**G**), or the scaffolding protein PSD95 (**J**). Bars= 5 μm.

(**B,E,H,K**) Quantitative analysis of density of immunofluorescently labeled puncta. In all hippocampal subfields, the density of puncta immunolabeled for GluA1 (**B**) and PSD95 (**K**)

was significantly lower in adult cKO mice (black bars) in comparison with that in adult floxed control mice (grey bars). In contrast, there were no differences between genotypes in density of GluA2 (**E**) or GluN1 (**H**). *p < 0.05, unpaired Student's t-test; n=8 per genotype, both sexes. For each region, values were normalized to those of the floxed control mice for that region.

(C,F,I,L) Quantitative analysis of sizes of immunofluorescently labeled puncta. GluA1 immunolabeled puncta were significantly smaller in all hippocampal subfields in cKO mice (**C**, black bars) in comparison with floxed control mice (**C**, grey bars). There were no differences in sizes of puncta immunolabeled for GluA2 (**F**), GluN1 (**I**) or PSD95 (**L**). *p < 0.05, unpaired Student's t-test; n=8 per genotype, both sexes. For each region, values were normalized to those of the floxed control mice for that region.

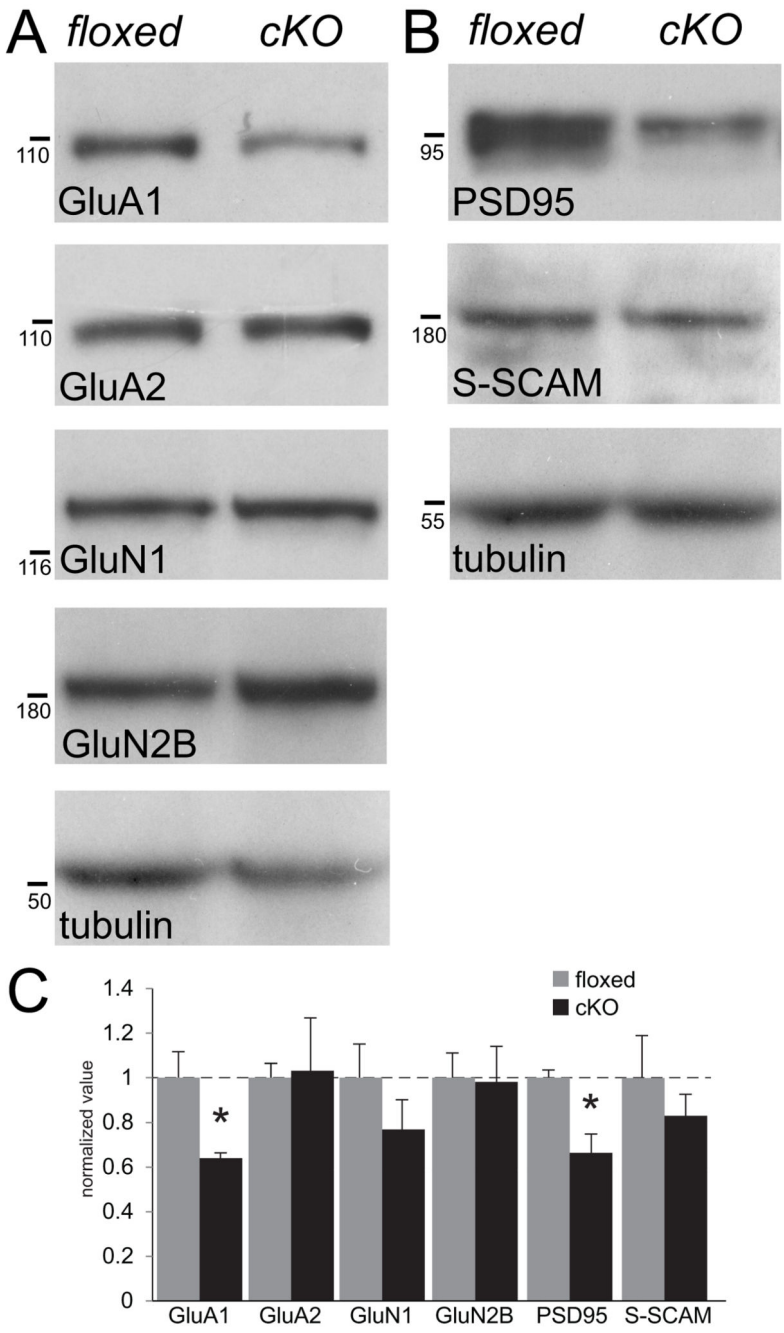

Fig. 6. Quantitative analysis of levels of AMPAR and NMDAR subunits and their scaffolding proteins in N-cadherin cKO hippocampus

(A and B) Representative immunoblots of synaptoneurosomes isolated from whole-hippocampus prepared from adult floxed and cKO mice showing diminished levels of GluA1 and its scaffolding protein PSD95, but no changes in levels of GluA2, its scaffolding protein S-SCAM/MAGI-2, or NMDAR subunits GluN1 or GluN2. Tubulin was used as a loading control. Numbers (on left) indicate approximate positions of molecular mass markers (kDa).

(C) Quantitative densitometric analysis of immunoblots of synaptoneurosomes. *p<0.05, n=3 mice per genotype, unpaired Student's t-test. For each molecule, values were normalized to those of the floxed control mice for that molecule.

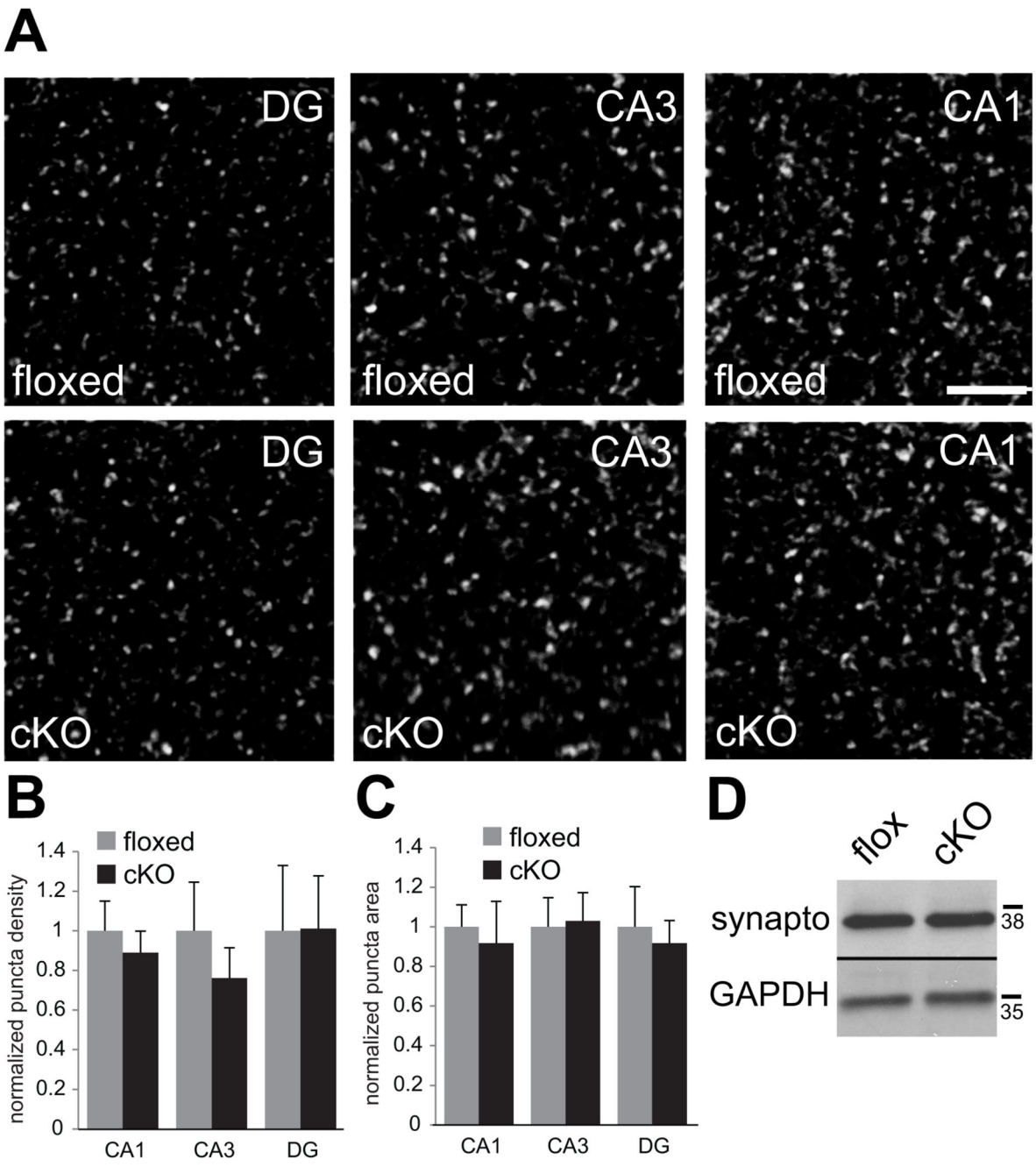

Fig. 7. No changes in levels or localization of presynaptic molecules in N-cadherin cKO mice

(A) Representative confocal images showing vGlut1/2 immunolabeling in the indicated subfields of hippocampus taken from adult floxed control mice (top row) or cKO mice (bottom row). Bar= 5 μm.

(B and C) Quantitative analysis of vGlut1/2 puncta density (B) and size (C). n=8 mice per genotype, both sexes ($p > 0.1$, unpaired Student's t-test). For each region, values were normalized to those of the floxed control mice for that region.

(D) Representative immunoblot of whole-hippocampal lysate showing similar levels of synaptophysin in floxed and cKO mice. GAPDH was used as a loading control. Numbers (on right) indicate approximate positions of molecular mass markers (kDa).

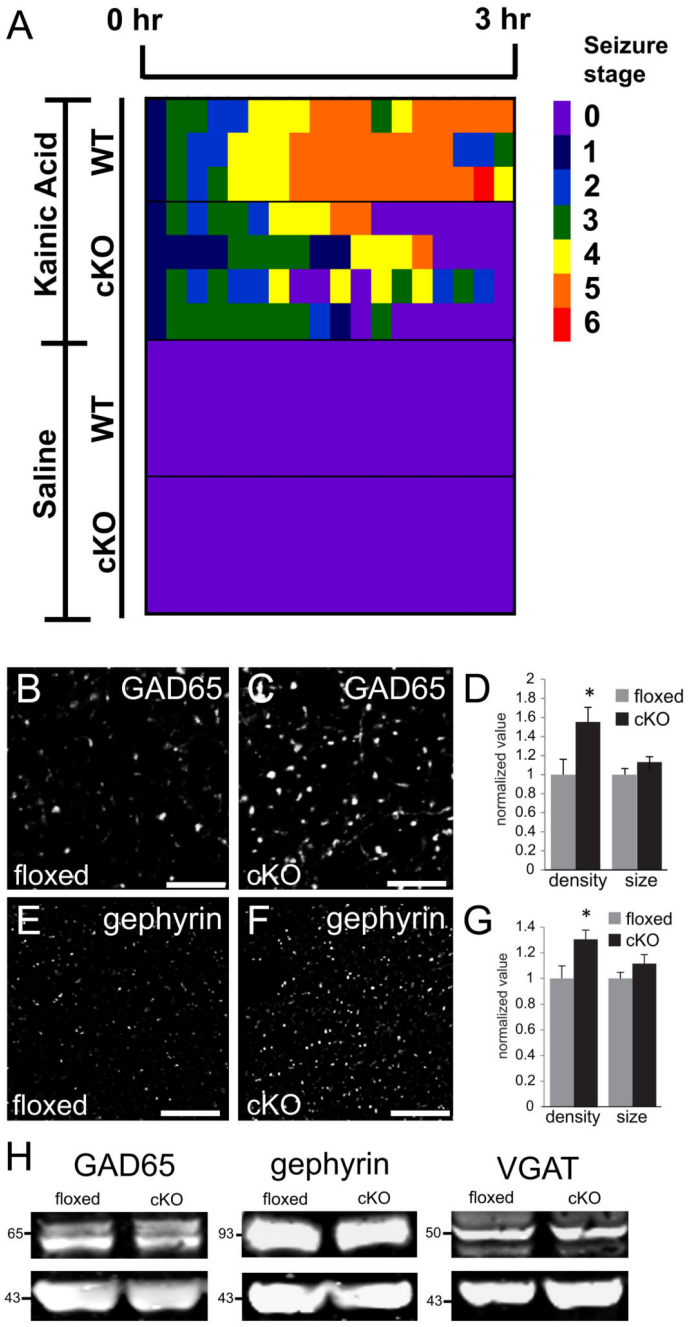

Fig. 8. Elevated density of GABA synapse markers and seizure threshold in N-cadherin cKO mice

(A) Pseudo-colored heat-map showing severity of behavioral seizures following injection of kainic acid (top maps) or saline (bottom maps) into cKO or wildtype (WT) mice. No animal displayed seizures following injection of saline. WT mice displayed a greater seizure severity profile (yellow-red) following kainic acid injection in comparison with cKO mice (green-yellow) over the 3-hr period of monitoring. Quantification of genotype differences in

seizure severity profiles is given in the text. See Materials and Methods for description of seizure stages (0-6) depicted in the heat-maps. n=3 male mice (WT) or 4 male mice (cKO). **(B-G)** Representative confocal images of immunolabeling for GAD65 (B,C) or gephyrin (E,F) and quantification of immunolabeled profiles (D, G) taken from CA1 stratum radiatum from an adult floxed control mice (B,E) or a cKO mouse (C,F). Quantification of immunolabeled profiles (D,G) shows a significant elevation in density of GAD65 and gephyrin puncta, but no changes in puncta size for either marker (n=4 mice per genotype, $p<0.05$, unpaired Student's t-test). Images were acquired from separate, single-labeled series of sections. Values for each condition were normalized to those of the floxed control mice. Bar= 5 μm.

(**H**) Immunoblots of synaptoneurosomes prepared from whole-hippocampal lysates taken from cKO or floxed control mice show no differences between genotypes in overall levels of GAD65, gephryin or VGAT. Actin (the lower blots of each pair) was used as a loading control. Numbers (on left) indicate approximate positions of molecular mass markers (kDa).

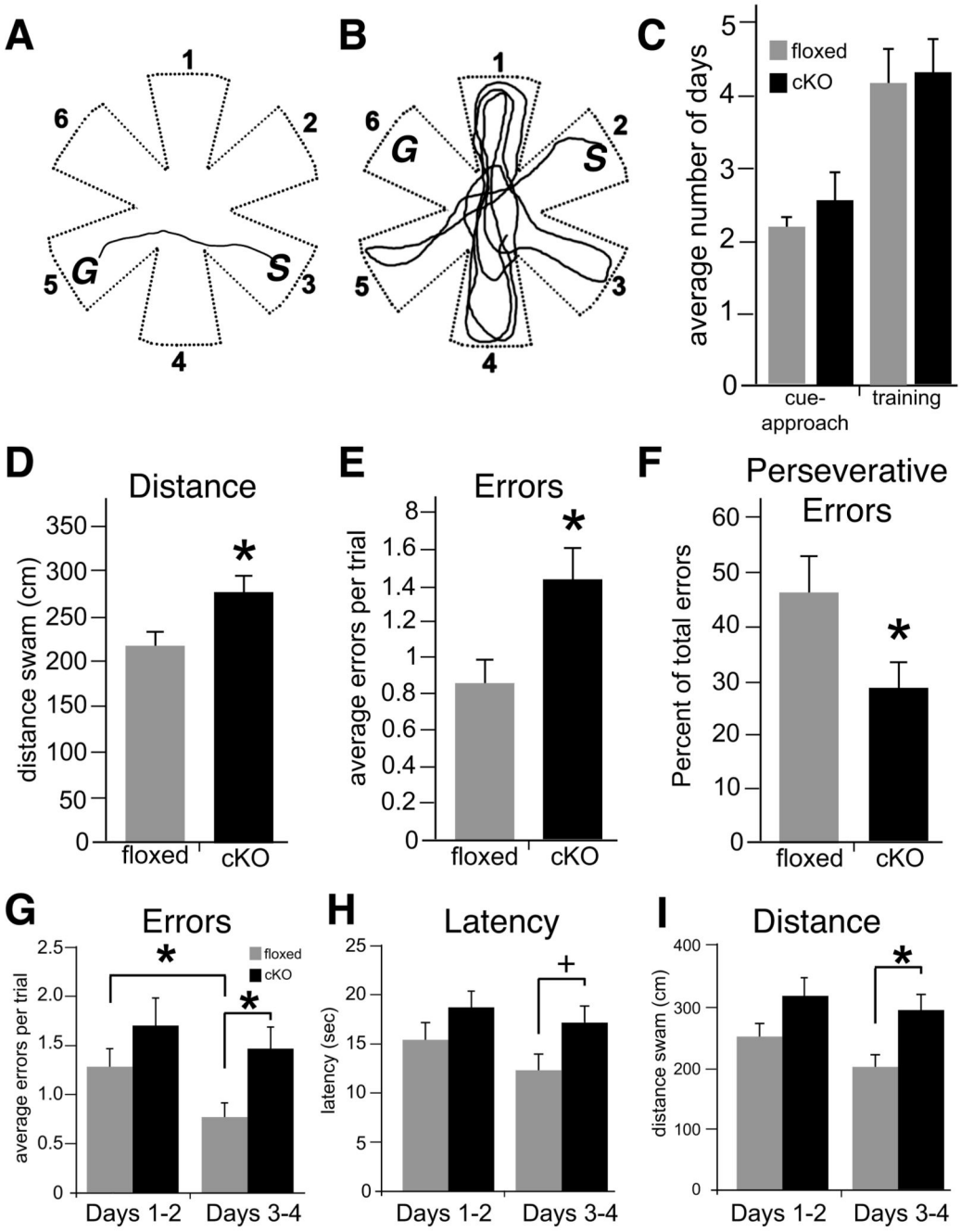

Fig. 9. Adult N-cadherin cKO mice display significant deficits in memory for spatial episodes

(A and B) Top-down view of the six-arm radial water maze showing representative trajectory (line) of a floxed control mouse (A) or a cKO mouse (B) on a match trial. Numbers mark each of the six arms of the maze. After the sample trial, the floxed control mouse swims directly from the Start arm (S, arm 3) to the correct Goal arm (G, arm 5), suggesting intact memory for the spatial cues used to encode the location of the escape platform. In contrast, the cKO mouse explores many incorrect arms and fails to find the location of the Goal arm (G, arm 6), indicating a failure of memory of the correct location.

(C) There were no differences between genotypes in the average number of days to reach criterion in cue-approach performance (left) nor in the training phase (right, unpaired Student's t-test).

(D-F) Quantitative measures of match-trial performance on the match-to-place version of the task. Measures include swim-path distance (D), number of errors (entry into non-goal arms, E) and perseverative errors (entry into the previous day's Goal arm, F). *$p<0.05$, n=13 cKO mice and 11 floxed control mice of either sex, unpaired Student's t-test).

(G-I) Average match-trial performance in the win-shift version of the task. Performance in this four-day task was divided into the first two days (days 1-2) and the last two days (days 3-4). There were no differences between genotypes in errors (entry into non-goal arms, G), latency to reach the platform (H) or total distance swam during the first two days of testing. However, floxed control mice committed significantly fewer errors during the last two days in comparison with their performance during the first two days (*$p < 0.01$), while the cKO mice failed to show any improvement ($p=0.24$). The cKO mice performed significantly worse than floxed control mice in all measures during days 3-4. *$p < 0.01$, $^{+}p < 0.05$, n=13 cKO mice and 11 floxed control mice of either sex, two-way repeated-measures ANOVA.

Table 1

Primary Antibodies

Antibody	Host, isotype	Immunogen	Source	Cat. #	Clone #
N-cadherin	Ms, IgG_1	aa 802-819 from Ms	BD Transduction Labs	610921	32/Ncadherin
β-catenin	Rb, IgG	fusion protein, full-length Hu	Millipore	AB19022	n/a
GluA1	Rb, IgG	extracellular domain, rat	Millipore	ABN241	n/a
GluA2	Ms, IgG_{2a}	aa 175-430 from rat	BD Pharmingen	556341	6C4
GluN1	Rb, IgG	C-terminal peptide from Hu	Millipore	AB9864R	1.17.2.6
GluN2B	Rb, IgG	aa 1437-1456 from Ms	Millipore	06-600	n/a
PSD-95	Ms, IgG_1	purified rat PSD-95	Thermo Scientific	MA1-046	7E3-1B8
pan-PSD-95	Ms, IgG_{2a}	purified rat PSD-95	Thermo Scientific	MA1-045	6G6-1C9
S-SCAM	Rb, IgG	aa 554-571	Sigma-Aldrich	SAB4503718	n/a
SynCAM-1	Chk, IgY	recombinant Fc-fusion	MBL International	CM004-3	3E1
gephyrin	Rb, IgG	synthetic peptide from rat	Millipore	AB5725	n/a
GAD65	Rb, IgG	synthetic peptide from Hu	Millipore	ABN101	n/a
VGAT	Ms, IgG_3	aa 75-87 from rat	Synaptic Systems	131 011	117G4
Synaptophysin	Ms, IgG_1	rat retina synaptosome	Sigma-Aldrich	S5768	SVP-38
vGlut 1	GP, IgG	peptide to vGlut1	Millipore	AB5905	n/a
vGlut2	GP, IgG	peptide to C-terminus	Millipore	AB2251	n/a
tubulin	Rb, IgG	aa 426-450 from Hu	Abcam	ab125267	n/a
actin	Ms, IgG_1	aa 50-70 from Chk	Millipore	MAB1501	C4
GAPDH	Rb, IgG	synthetic peptide from Hu	Trevigen	2275-PC-1	n/a

Chk, chicken; GP, guinea-pig; Hu, human; Ms, mouse; Rb, rabbit; aa, amino acid